Salience of Haptic Features

for Interactive Behavior Classification in

Physical Human-Human/Robot Collaboration

by

Zaid Rasim Mohammed Al-Saadi

A Dissertation Submitted to the
Graduate School of Sciences and Engineering
in Partial Fulfillment of the Requirements for

the Degree of

Doctor of Philosophy

in

Mechanical Engineering

KOÇ ÜNİVERSİTESİ

April 24, 2023

Salience of Haptic Features
for Interactive Behavior Classification in
Physical Human-Human/Robot Collaboration

Koç University
Graduate School of Sciences and Engineering

This is to certify that I have examined this copy of a doctoral dissertation by

Zaid Rasim Mohammed Al-Saadi

and have found that it is complete and satisfactory in all respects,
and that any and all revisions required by the final
examining committee have been made.

Committee Members:

____
Prof. Çağatay Başdogan (Advisor)

____
Asst. Prof. Ayşe Küçükyılmaz (Co-advisor)

____
Prof. Murat Sözer

____
Prof. Duygun Erol Barkana

____
Assoc. Prof. Mehmet Dogar

____
Asst. Prof. Yusuf Aydın

Date: ________________________________

To my beloved family

ABSTRACT

In recent years, a considerable amount of research has been directed toward designing robots to cooperate with humans in daily activities that require close physical interaction. One particular area of interest is collaborative object transportation, where human dyads would rely heavily on haptic sensations to coordinate their actions.

Humans are sensitive to interactive behaviors during joint action, and can leverage haptic cues (i.e., the forces they apply and sense through their interactions with the manipulated object) to easily distinguish between interaction states, such as harmony and conflict. Such discrimination between interaction states is currently missing in physical human-robot interaction (pHRI), and collaboration can be improved by making the robot proactive against changes in interaction behaviors.

We trust that understanding physical human-human interactions (pHHI) is crucial to implement a robotic system that is able to classify dyadic interactive behaviors. This dissertation is an effort to provide insight into the inherently important role of haptics in differentiating distinct interaction behavior classes during the collaboration of two physically-linked partners. To the best of our knowledge, ours is the first study to design interaction-specific haptic features to improve identification of conflict-related pHHI behaviors in physical co-manipulation. This haptic information works as a basis in pHRI to enable proactive robotic partners that can accommodate varying interactive behaviors.

In the first part of this dissertation, we explore the prominence of haptic data to extract information about underlying interaction patterns within physical human-human interaction (pHHI). We work on a joint object transportation scenario involving two human partners, and show that haptic features, based on force/torque information, suffice to identify human interactive behavior patterns. We categorize the interaction into four discrete behavior classes. These classes describe whether the partners work in harmony or face conflicts while jointly transporting an object through translational or rotational movements. In our experimental study, we collect data from 12 human dyads and verify

the salience of haptic features by achieving a correct classification rate over 91% using a Random Forest classifier.

The second part of this dissertation proposes a machine learning (ML) approach to detect and resolve motion conflicts that may occur between a human and a proactive robot during the execution of a collaborative task. Our approach aims to distinguish harmonious and conflicting behaviors by looking at dyadic interaction patterns rather than inferring solely about the individual state of the human partner. In doing so, we challenge the traditionally adopted dualistic attitude in physical HRI, which considers the human and the robot as distinct and separable entities, and instead, consider the kinesthetic information generated through the teamwork to describe the interactive quality of collaboration. We demonstrate that features derived from haptic (force/torque) data are sufficient to classify if the human and the robot harmoniously manipulate the object or they face a conflict. A conflict resolution strategy is implemented to get the robotic partner to proactively contribute to the task via online trajectory planning whenever interactive motion patterns are harmonious, and to follow the human lead when a conflict is detected. An admittance controller regulates the physical interaction between the human and the robot during the task. This enables the robot to follow the human passively when there is a conflict. An artificial potential field approach is used to make the robot proactive when partners work in harmony. An experimental study is designed to create scenarios involving harmonious and conflicting interactions between human and robot partners during the collaborative manipulation of an object, and to create a dataset to train and test our ML model. The results of the study show that ML successfully detects the conflicts and our conflict resolution mechanism reduces the human force and effort significantly compared to the case of a passive robot that always follows the human partner and a proactive robot that cannot resolve conflicts.

ÖZETÇE

Son yıllarda, yakın fiziksel etkileşim gerektiren günlük aktivitelerde insanlarla işbirliği yapacak robotlar tasarlamaya yönelik önemli miktarda araştırma yapılmıştır. Bu alanda bir araştırma alanı, insan ortakların eylemlerini koordine etmek için ağırlıklı olarak dokunsal duyuya güvendiği işbirlikçi nesne taşımacılığıdır.

İnsanlar, ortak eylem sırasında etkileşimli davranışlara karşı hassastır ve uyum ve çatışma gibi etkileşim durumlarını kolayca ayırt etmek için dokunsal ipuçlarından (yani, uyguladıkları ve manipüle edilen nesneyle etkileşimleri yoluyla algıladıkları kuvvetler / torklar) yararlanabilirler. Etkileşim durumları arasındaki bu tür bir ayrımın tespiti, fiziksel insan-robot etkileşiminde (pHRI) şu anda eksiktir ve etkileşim davranışlarındaki değişikliklere karşı robotu proaktif hale getirerek işbirliğini güclendirebilir.

Fiziksel insan-insan etkileşimlerini (pHHI) anlamanın, insan-robot etkileşimterini sınıflandırabilen bir yapay zeka sistemi için çok önemli olduğuna inanıyoruz. Bu tez, fiziksel olarak birbirine bağlı iki ortağın işbirliği sırasında farklı etkileşim davranış sınıflarını ayırt etmede dokunsal algının işin doğası gereği önemli olan rolüne ilişkin içgörü sağlama çabasıdır. Bildiğimiz kadarıyla, bu çalışma fiziksel birlikte manipülasyonda çatışmayla ilgili pHHI davranışlarının tanımlanmasını iyileştirmek için etkileşime özgü dokunsal özellikler tasarlayan ilk çalışmadır. Bu dokunsal bilgi, çeşitli etkileşimli davranışları barındırabilen proaktif robotik ortakları etkinleştirmek için pHRI'de bir temel olarak çalışır.

Bu tezin ilk bölümünde, fiziksel insan-insan etkileşimi (pHHI) içindeki etkileşim kalıpları hakkında bilgi çıkarmak için dokunsal verilerin önemini araştırıyoruz. İki insan ortağı içeren ortak bir nesne taşıma senaryosu üzerinde çalışıyoruz ve kuvvet/tork bilgisine dayalı dokunsal özelliklerin, insan etkileşimli davranış kalıplarını tanımlamaya yeterli olduğunu gösteriyoruz. Etkileşimi dört ayrı davranış sınıfına ayırıyoruz. Bu sınıflar, ortakların bir nesneyi öteleme veya dönme hareketleriyle birlikte taşırken uyum içinde çalışıp çalışmadıklarını veya çatışmalarla karşılaşıp karşılaşmadıklarını açıklar. Deneysel bir çalışmada, 12 insan çiftinden veri topluyoruz ve bir Random Forest sınıflandırıcı kullanarak 91% in üzerinde doğru bir sınıflandırma oranı elde ederek dokunsal özelliklerin belirginliğini doğruluyoruz.

Bu tezin ikinci kısmı, işbirlikçi bir görevin yürütülmesi sırasında bir insan ile proaktif bir robot arasında meydana gelebilecek hareket çatışmalarını tespit etmek ve çözmek için bir makine öğrenimi (ML) yaklaşımı önermektedir. Yaklaşımımız, yalnızca insan partnerin bireysel durumu hakkında çıkarım yapmak yerine ikili etkileşim modellerine bakarak uyumlu ve çelişkili davranışları ayırt etmeyi amaçlamaktadır. Bunu yaparken, insan ve robotu ayrı ve ayrılabilir varlıklar olarak gören ve bunun yerine işbirliğinin etkileşimli kalitesini tanımlamak için ekip çalışması yoluyla üretilen kinestetik bilgileri dikkate alan fiziksel HRI'da geleneksel olarak benimsenen dualistik tutuma meydan okuyoruz. Dokunsal (kuvvet/tork) verilerinden türetilen özelliklerin, insan ve robotun nesneyi uyumlu bir şekilde manipüle edip etmediğini veya bir çatışmayla karşı karşıya olup olmadığını sınıflandırmak için yeterli olduğunu gösteriyoruz. Etkileşimli hareket kalıpları uyumlu olduğunda robot ortağının çevrimiçi yörünge planlaması yoluyla göreve proaktif olarak katkıda bulunmasını ve bir çatışma algılandığında insan liderliğini takip etmesini sağlamak için bir çatışma çözme stratejisi uygulanır. Kabul denetleyicisi, görev sırasında insan ve robot arasındaki fiziksel etkileşimi düzenler. Bu, bir çatışma olduğunda robotun insanı pasif olarak takip etmesini sağlar. Ortaklar uyum içinde çalışırken robotu proaktif hale getirmek için yapay bir potansiyel alan yaklaşımı kullanılır. Deneysel bir çalışma, bir nesnenin işbirlikçi manipülasyonu sırasında insan ve robot ortakları arasındaki uyumlu ve çelişkili etkileşimleri içeren senaryolar oluşturmak ve makine öğrenimi modelimizi eğitmek ve test etmek için bir veri kümesi oluşturmak üzere tasarlanmıştır. Çalışmanın sonuçları, makine öğreniminin çatışmaları başarılı bir şekilde tespit ettiğini ve çatışma çözme mekanizmamızın, her zaman insan ortağını takip eden pasif bir robot ve çatışmaları çözemeyen proaktif bir robot durumuna kıyasla insan gücünü ve çabasını önemli ölçüde azalttığını göstermektedir.

ACKNOWLEDGEMENTS

First and foremost, my most profound appreciation goes to Professor Çağatay Başdogan, my research advisor, for his time, effort, and understanding in helping me succeed in my studies. His vast wisdom and wealth of experience have inspired me throughout my studies and allowed me to grow as a research scientist. I would like to express my deepest appreciation to him for his work and dedication to research.

I would like to acknowledge my indebtedness and render my warmest thanks to my research co-advisor Professor Ayşe Kuçukyilmaz. She has been a tremendous mentor for me and always encouraged me to look deeper into the problems with a creative spirit. Her advice, brilliant comments, and suggestions have been invaluable.

I would like to thank Dr. Yusuf Aydin for being a companion for me during my study and for the practical solutions he offered, and all the assistance whenever I needed it.

I would like to also express my gratitude to Professor Murat Sözer for being in the thesis monitoring committee and for his valuable criticism, suggestions, and guidance for my dissertation.

I can never thank enough my incredible family. Words cannot express how grateful I am to my dear father and dear mother for all of the sacrifices that they've made on my behalf. their prayers for me were what sustained me thus far. I want to thank my brother Ahmed, and my sisters Hind and Rand. They always believed in me and supported me through my studies and my life. I could not have undertaken this journey without their support and encouragement.

I would also like to thank my beloved wife, Dhuha, for her love and constant support. Her presence gave me a feeling of wholeness. I believe this journey took a toll on her as well. I am forever thankful to her for being a part of my life. Furthermore, great thanks go for my small angel, Miral, and my son, Aser, who have been the light of my life for the last few years and who have given me the extra strength and motivation to get things done.

I would like to thank my dear friend Yahya Al-Qaysi, for his endless support and understanding throughout this process. I am forever in his debt for how much he has taught me.

I want to express my gratitude to my colleagues Berk Güler and Feras Kiki for their support, assistance, and motivation. It was a privilege to know and share time with all former and current members of the Robotics and Mechatronics Laboratory (RML): Dr. Bushra Sadia, Dr. Khurram Saleem, Dr. Özan Çaldıran, Dr. Ömer Şirin, Dr. Yasemin Vardar, Dr. Ezgi Senem Emgin, Utku Erdem, Milad Jamalzadeh, Alireza Madani, Mohammad Reza Chehrezad, Doğanay Şirintuna, Utku Erdem, İdil Özdamar, Easa Aliabbasi, Berke Ataseven, Pouya Pourakbarian Niaz, Jahangier Ahmad, Sara Hamdan, Riaz Minhas, and Muhammad Muzammil.

I want to express my gratitude to University of Baghdad for financially supporting me through my Ph.D. studies.

TABLE OF CONTENTS

LIST OF TABLES

LIST OF FIGURES

NOMENCLATURE

Acronyms

ANN	artificial neural network
ANOVA	analysis of variance
APF	artificial potential field
ArUco	augmented reality university of cordoba
BER	balanced error rate
CD	conflict in target direction
CP	conflict in parking location
CR	conflicting rotation
CT	conflicting translation
DoF	degree of freedom
EB	expected behavior
ELM	extreme learning machine
EMG	electromyography
ES	experimental scenario
F/T	force/torque
FPB	force plane-based feature set
FSB	force space-based feature set
HR	harmonious rotation
HT	harmonious translation
IMU	inertial measurement unit
L1O	leave-one-out cross validation
LSTM	long short-term memory
MDI	mean decrease impurity
ML	machine learning
pHHI	physical human-human interaction
pHRI	physical human-robot interaction
PM	primitive motion

PP	processed predictions
RBF	radial basis function
RP	raw predictions
Sc	experimenter's scenarios
SD	standard deviation
TPB	torque plane-based feature set
TS	training scenario
TSB	torque space-based feature set
WH	working in harmony
WPB	wrench plane-based feature set
WSB	wrench space-based feature set

List of symbols

D	put the manipulated object down
d_s	distance threshold around object's starting position
d_t	positive constant to define a catchment area around the target
E	experimenter
F_E^*	effective force applied by the experimenter on the manipulated object
$F_{E_A}^*$	effective force applied by experimenter on plane A
F_S^*	effective force applied by the subject on the manipulated object
$F_{S_A}^*$	effective force applied by subject on plane A
F_H^{AVE}	average force applied by subject
F_{ATT}	attractive force
F_E	force vector exerted by the experimenter on the manipulated object
F_{E_A}	force vector exerted by the experimenter on plane A
F_H	force applied by human partner on the manipulated object
F_{NORMAL}	force normal component
F_S	force vector exerted by the subject on the manipulated object

F_{S_A}	force vector exerted by the subject on plane A
F_{SUM}	resultant net force vector acting on the manipulated object
F_{SUM_A}	net force vector applied on the manipulated object by the partners on plane A
F_T	total force vector
$F_T(s)$	laplace transformations of the total force
K_A	admittance gain
l	euclidian distance between the object's starting position vector and the estimated target
$M_{E_K}^{\tau}$	individual torque efficiency
M_{NE}^{τ}	negotiation torque efficiency
M_S^{τ}	similarity of torques
M_{TE}^{τ}	team torque efficiency
m	scaling constant
$M_{E_K}^{F}$	individual force efficiency
M_{NE}^{F}	negotiation force efficiency
M_S^{F}	similarity of forces
M_{TE}^{F}	team force efficiency
n	size of sliding buffer
P^{AVE}	average power consumed by the human
Q	current position vector of the manipulated object with respect to the robot base frame
Q_{START}	manipulated object's starting position vector
Q_{TARGET}	target position vector with respect to the robot base frame
R_x^+	rotate the manipulated object counterclockwise about the *x*-axis
R_x^-	rotate the manipulated object clockwise about *x*-axis
R	rotation
S	subject
T_y^+	translate the manipulated object along the *y*-axis
T_z^-	translate the manipulated object along the negative *z*-axis
T	translation

TCT	task completion time
t_f	ending time of the trial
t_i	starting time of the trial
U	lift the manipulated object up
$U(Q)$	total potential field
$U_{ATT}(Q)$	attractive potential field
$U_{REP}(Q)$	repulsive potential field
V	manipulated object's velocity
V^{AVE}	average velocity of the manipulated object
V_{REF}	reference velocity
$V_{REF}(s)$	laplace transformations of the reference velocity
W_H	wrench applied by human on the manipulated object
W_R	wrench applied by robot on the manipulated object
$Y(s)$	transfer function model of the admittance controller
δ	force cooperation index
θ	angle between the human force vector and the x-axis of robot
θ_{AVE}	average value of angles between the human force vector and the x-axis of robot
θ_{THR}	threshold value of angle between the human force vector and the x-axis of robot
ξ	positive constant scaling factor
$\rho_{START}(Q)$	manipulated object's euclidean distance to start position
$\rho_{TARGET}(Q)$	manipulated object's euclidean distance to target
τ_E^*	effective torque applied by the experimenter on the manipulated object
$\tau_{E_A}^*$	effective torque applied by experimenter about the axis perpendicular to the plane A
τ_S^*	effective torque applied by the subject on the manipulated object
$\tau_{S_A}^*$	effective torque applied by subject about the axis perpendicular to the plane A
τ	total torque vector

τ_A	time constant
τ_E	torque vector exerted by the experimenter on the manipulated object
τ_{E_A}	torque exerted by the experimenter about the axis perpendicular to the plane A
τ_S	torque vector exerted by the subject on the manipulated object
τ_{S_A}	torque vector exerted by the subject about the axis perpendicular to the plane A
τ_{SUM}	net torque vector applied on the manipulated object
τ_{SUM_A}	net torque applied by the partners about the axis perpendicular to the plane A
τ_{SUM_X}	net torque applied on the manipulated object about the x-axis
τ_{SUM_Y}	net torque applied on the manipulated object about the y-axis
τ_{SUM_Z}	net torque applied on the manipulated object about the z-axis
τ^c	computed torque vector
τ_x^c	computed torque about the x-axis
τ_y^c	computed torque about the y-axis
τ_z^c	computed torque about the z-axis
τ^m	measured torque vector
τ_x^m	measured torque about the x-axis
τ_y^m	measured torque about the y-axis
τ_z^m	measured torque about the z-axis

Chapter 1

INTRODUCTION

Collaborative robots have emerged during the last two decades due to the advancements in hardware (e.g., lightweight design, built-in force/torque sensing) and software (user-friendly interfaces, the introduction of artificial intelligence techniques, etc.). These enhancements have allowed robots to act near humans in activities through indirect interaction [1, 2] or within direct physical contact with humans [3, 4].

A collaborative robot can proactively assist the human partner during the task while bearing the weight of the manipulated object to reduce her/his effort. Moreover, as more sophisticated AI techniques are expected to be integrated into such robotic systems, robots collaborating with humans are expected to have their own intentions. In such a scenario, due to the agreement/disagreement between human and robot intentions, different interaction behaviors arise. For instance, consider a robot that proactively contributes to a co-manipulation task performed with a human partner. If they have a joint intention to manipulate the object toward the same target, they will work harmoniously with minimal conflict. This harmonious interaction enables human to spend less effort during the task. However, if human suddenly changes the target location by altering the direction of movement or parking the manipulated object before/after the initial target location while the robot keeps moving toward it, conflicting behaviors arise. Such behaviors create undesired interactions, which make the task more tiring for the human partner unless the robot recognizes these conflicts and reacts to resolve them.

To this end, we believe that understanding how two human partners physically interact to manipulate an object relying on haptic clues is essential to design a robotic system that can classify dyadic interactive behaviors. Haptics provides a natural and intuitive channel of communication during the interaction of human-human in complex physical tasks, such as joint object transportation. However, despite the utmost importance of touch in physical interactions, the use of haptics (i.e., force and torque) is under-represented when developing intelligent systems.

This dissertation is an effort to explore the utility of haptics in capturing interaction characteristics in physical human-human interaction (pHHI) as a motivation to build a robotic system that can proactively cooperate with human partners in physical human-robot interaction (pHRI). In particular, in the first part of this dissertation, we seek evidence that harmonious and conflicting behavior patterns in pHHI can be recognized using haptic information alone. The findings of our pHHI study work as a basis for the second part of this dissertation to enable robotic partners in pHRI to proactively collaborate with human partners by accommodating the varying interactive behaviors that emerge during the collaboration.

In our approach, we define our task as an object manipulation task where two partners are always needed to hold the object and transfer it from one position to another. Moreover, we assume that there are always two force sensors (one for each partner) to record the haptic data applied on the object.

1.1 Related Work

We review the earlier studies in two groups: haptics in human-human/robot interaction and human intentions in physical human-robot interaction.

1.1.1 Haptics in Human-Human/Robot Interaction

Recent literature indicates that haptic feedback plays an important role in improving the task performance of interacting partners in virtual environments [5]–[11], when working with real robots [12], [13], and in pHHI [14].

In addition to performance benefits, haptics has a communicative function. Takagi et al. [11] explored the effect of haptic communication on dyads' performance in a dynamic target tracking task. They suggested that the coupling dynamics may determine the amount of information that can be communicated among physically interacting partners. Mielke et al. [14] showed that when two humans collaboratively move an object, lateral movements were triggered by a specific force profile applied by the leader. Using this force profile, the intention for future motion could be predicted. Later, the same group showed that linear and angular velocity of the co-manipulated object can be used to accurately estimate the human motion intention (i.e., translation vs. rotation) [15]. Parastegari et al. [13] designed a controller for robot-to-human handover, where they used the pulling force applied on the object, the object acceleration, and the relative motion between the object and the robot hand, to achieve smooth and safe handover.

In human studies, haptics has been used to assess the performance of dyad in manipulation tasks. Noohi and Žefran [16] investigated the quality of collaboration in physical human-human interaction while two partners lift an object vertically. They proposed a set of quantitative metrics that evaluate the performance of haptically-coupled subjects, and cross-validated those metrics with the subjects' self-assessments. These metrics were valid for a 1D translation task, and assessed the performance of the partners in terms of the efficiencies of individuals, the team, and their negotiation, as well as the similarity of forces. In this study, we designed our features through inspiration from this study. We modified these metrics to support a 6-DoF task by reformulating the metrics to handle torques as well as forces in the 3D Cartesian space.

Another interesting observation arising from human studies is about role allocations between partners during dyadic interaction [17]. Reed and Peshkin [18] observed that when two human partners perform a dyadic target acquisition task, two opposing roles, responsible for accelerating or decelerating the task, were adopted by collaborating humans. Stefanov et al. [19] also observed two roles in human-human haptic interaction, namely the executor and the conductor of the task. Both studies identified the roles regarding interaction forces and velocities. On the other hand, Takagi et al. [20] examined rigidly coupled dyadic reaching movements. Although their study showed that the dyads did not coordinate during joint reaching movements towards the same target, the collaborating partners still displayed “accelerating” versus “decelerating” roles. However, they explained these acceleration/deceleration roles by the speed mismatch between the partners and the differences in their movement reaction times.

Even though the literature is rich in terms of defining human intentions and partner roles in dyadic interaction, there are only a few studies that focus on collaborative tasks as an attempt to define possible interaction patterns. Melendez-Calderon et al. [21] defined five human interaction patterns for a tracking task. This study provided static and task-dependent roles. A rule-based quantitative classification technique, depending on the interaction torques and EMG recordings from partners, was proposed to identify these roles and discuss their efficiencies for specific tasks. Jarrass´e et al. [22] presented a comprehensive taxonomy of interactive behaviors, namely competition, collaboration, and cooperation. They proposed a utility-based game theoretic approach to describe and implement interactive behaviors, where cost functions are defined to distinguish between interaction classes. This approach was later demonstrated on a simple reaching task with a robot [23]. Agravante et al. [24] introduced a taxonomy for collaborative object transportation by classifying the grasp types and the relative pose between the agents. They decomposed a complex transportation task into subtasks and used a finite state machine to program a robot to perform the task collaboratively with a human partner. Madan et al. [25] proposed a hierarchical taxonomy for pHHI, defining three main classes of collaborative interaction types, namely harmonious, conflicting, and neutral behaviors. In contrast to the aforementioned studies, the taxonomy in [25] looks at general interaction states and provides a simpler characterization for physical collaboration; hence, [25] will be used in this study to define the behavior classes.

Our hypothesis is that haptic-related features would be sufficient to distinguish between interactive behavior patterns without the need to include the kinematic information, eliminating the need to track the manipulated object. In [25], Madan et al. investigated the use of raw interaction data and extracted features by processing the partners' applied forces and the manipulated object's velocity from annotated data. Later, Kucukyilmaz and Issak [26] proposed an online feature extraction method and demonstrated its use for identifying interaction patterns in real-time collaboration using similar features. In both studies, they observed that raw haptic data were insufficient to achieve good classification rates and the object pose information was needed. Hence, in the first part of this dissertation, we utilize richer haptic features derived from raw data to improve the accuracy in classifying interaction behaviors without a need for object pose information. Selected features isolate haptics-related information and aim to demonstrate the prominence and sufficiency of haptics in explaining interaction states during pHHI.

1.1.2 Human Intentions in Physical Human-Robot Interaction

In physical human-robot interaction (pHRI), a considerable amount of research has been directed toward detecting human intentions to regulate the interactions between human and robot. Many of the earlier studies implemented rule-based methods, while more recent ones employed ML techniques. In this regard, we review the existing literature based on these two groups of studies.

In rule-based approaches, typically a set of rules are defined, based on thresholds over kinematic or kinetic interaction variables to detect human movement intentions. Wojtara et al. [27] implemented an interaction controller that allows a robot to follow the human partner's movement during a collaborative manipulation task based on the forces applied by the human on the object and the position of the human's grasp point. Other studies utilized velocity and human force [28], velocity and derivative of human force [29], velocity and acceleration [30], and velocity, human force, and its derivative [31] to predict human intentions to adjust the parameters of an interaction controller for the robot during a collaborative manipulation task.

Rule-based approaches are also used to estimate human intention to exchange roles, such as between leadership and followership. For example, Oguz et al. [32] and Kucukyilmaz et al. [33] proposed mechanisms for dynamic role exchanges between the human and the robot during collaborative haptic interaction tasks. In these studies, the authors inferred human intentions based on the forces applied on the manipulated object by the human to adjust the robot's role in the collaborative task. Later, Mörtl et al. [34] extended these methods to develop a rule-based strategy where robot and human partners could dynamically exchange their roles and adjust their contributions to the task based on the forces during a table co-manipulation task. Khoramshahi and Billard [35, 36] proposed dynamical system approaches in pHRI using human intended motion velocity to switch between different tasks, and to change robot's role between a stiff leader or a compliant follower to a human partner. Although these works demonstrate switching behaviors between active/passive roles, they do not perform harmony/conflict detection as done in this study.

The emergence of machine/deep learning techniques has encouraged the researchers in pHRI to detect human intentions using data/model-driven approaches. Townsend et al. [37] trained an artificial neural network (ANN) model to predict the future human velocity based on the past velocity and acceleration using the data collected from human dyads in a co-manipulation task. This model was then validated on a table carrying task executed by a human and robot dyad. Whitsell and Artemiadis [38] presented a controller that enables humans to take the leadership on any axis they desire while manipulating an object with a robot. They utilized force and torque data as inputs to a reinforcement learning algorithm to predict the value of future rewards to activate or deactivate the robot in the desired axis. Ge et al. [39] used the force, velocity, and position measured at the interaction point between the robot arm and human upper limb as inputs to an ANN model to estimate human motion intention which is defined as the desired trajectory of human upper limb. Based on this model, Li and Ge [40] developed an adaptive interaction controller that utilized the estimated human motion intention to enable a robot to actively collaborate with a human partner instead of passively following her/his forces. Guler et al. [41] trained an ANN classifier to detect the subtasks intended to be executed by the human operator during a collaborative drilling task. They adapted the control parameters of an interaction controller of robot based on the detected subtask to improve task efficiency. The results of the experimental study conducted with 12 participants showed that the proposed subtask classifier reduces the human effort by 20% and drilling oscillations by 25%. Lu et al. [42] utilized a LSTM model to estimate human motion intention as the desired trajectory based on human limb dynamics in a human-robot collaborative task. Moreover, a reinforcement learning algorithm was implemented to adjust one of the parameters of an interaction controller in real-time based on the estimated human intention. Ly et al. [43] trained a Deep Q-Network to estimate human intentions to reach pre-learned motion trajectories and provided adaptive haptic guidance on a robotic sorting task. Chien et al. [44] proposed a fuzzy RBF approach to estimate human hand impedance and an ANN model to estimate human motion intention, which is used to generate a reference trajectory, to compute the compensation force that assists the robot in following the intended trajectory. Wang et al. [45] proposed an approach to estimate human intention in human-robot hand-over tasks. In their approach, they utilized an inertial measurement unit (IMU) and eight EMG sensors attached to the human forearm to measure arm motion along with muscle activity. These data were used as inputs to the extreme learning machine (ELM) algorithm to predict human hand-over intention. Sirintuna et al. [46] used EMG signals to detect the movement direction intended by human using an ANN model to constrain the movements in other directions using an interaction controller. They showed that this approach reduces the undesired motion errors during a collaborative positioning task executed with a robot.

The above studies focused on inferring human intentions to regulate the human-robot interactions. However, in the foreseeable future, as more sophisticated AI techniques are expected to be integrated into robotic systems, robots collaborating with humans are expected to have their own intentions. In such a scenario, if the intentions of a robot do not match those of the human, there will be motion conflicts [47]. Such undesired interaction behaviors should be recognized by robot partner and behave accordingly.

Consequently, In the second part of this dissertation, we aim to transfer the knowledge gained from human-human study (first part of this dissertation) to develop a system that identify the interaction behaviors in real-time during a physical human-robot interaction pHRI. To this end, we trust that the identification and resolution of conflicts is a key skill that a robot needs to be equipped with to execute more intuitive co-manipulation tasks with a human. We utilize features extracted from haptic data only to build a ML classifier that enables the robot to predict interaction behaviors and resolve conflicts when necessary. In our approach, the robot contributes to the co-manipulation task proactively when the partners work in harmony or follows the human when there is a conflict in the partners' intentions. We show that the proposed approach reduces the human force and effort significantly compared to the case of a passive robot that always follows human partner and a proactive robot that cannot resolve conflicts.

1.2 Outline

The rest of this dissertation is organized as follows:

Chapter 2 presents a novel haptic feature set for the classification of interactive motor behaviors in collaborative object transfer. Section 2.1 introduces the human-human object manipulation experiment, where the experimental apparatus and data collection, the interaction patterns, the experimental scenarios, participants and protocol, and data segmentation are reported. Section 2.2 presents an in-depth investigation of the force/torque patterns encountered in the proposed scenarios. The haptic-related metrics are introduced in Section 2.3. Section 2.4 presents, in details, the feature extraction and ML classifier design. Results and discussion are summarized in Section 2.5.

The proposed approach that enables the robot to detect the dyadic interaction behaviors and resolve the conflict emerges during the execution of the co-manipulation task is introduced in Chapter 3. Our approach that enables the robot to cooperate with human partner, hardware setup, control architecture, and trajectory generation are reported in Section 3.1. Section 3.2 presents the pHRI experiment (i.e., the training and validation scenarios), participants and protocol, haptic features and classifier design, and results and discussions.

Finally, Conclusions and future research directions are provided in Chapter 4.

Chapter 2:

A NOVEL HAPTIC FEATURE SET FOR THE CLASSIFICATION OF INTERACTIVE MOTOR BEHAVIORS IN COLLABORATIVE OBJECT TRANSFER

In this chapter, we report evidence that harmonious and conflicting behavior patterns in pHHI can be recognized using metrics derived from haptic information alone. For this purpose, we present an experimental study with 12 subjects in a 6-DoF object manipulation task, as shown in Figure 2.1. Six task scenarios are designed, in each of which at least two of four specific interaction behavior patterns are generated:

1) Harmonious Translation **(HT)**.
2) Conflicting Translation **(CT)**.
3) Harmonious Rotation **(HR)**.
4) Conflicting Rotation **(CR)**.

In order to distinguish between these interaction classes, we define features based on the metrics devised by Noohi and Žefran to quantify the collaboration quality during a dyadic manipulation task [16]. As these metrics are originally defined for a vertical translation task, they do not capture torque-related information, which is essential to describe rotational motion in a 6-DoF task. To address this, we combine force and torque information and design wrench-based metrics.

For the classification of interaction behaviors, we train a Random Forest classifier [48]. Our results indicate that the trained classifier achieves a correct classification rate over 91%, underlining the prominent influence of haptics in distinguishing between interactive behavior classes.

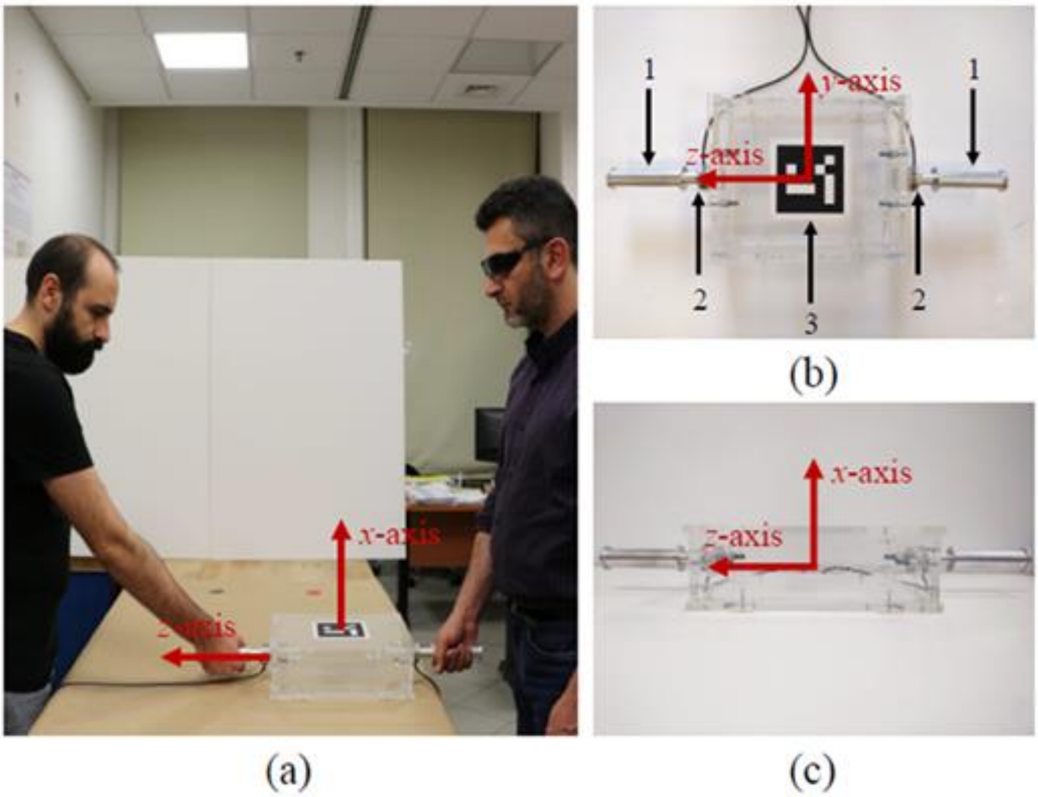

Figure 2.1: (a) Two humans cooperate to manipulate an object from one location to another. (b) and (c) are the top and the front views of the manipulated object, respectively. The object coordinate frame is shown in red. The numbers 1, 2, and 3 in (b) highlight the handles, the F/T sensors, and the ArUco marker, respectively.

2.1 Experiment

An experiment is designed to create a dataset of pHHI behaviors. The experimental task requires two human partners to collaborate in order to lift, move, and place an object to a target configuration through translational and rotational movements. This section describes the experimental setup and the protocol and details the data collection and preparation process.

2.1.1 Experimental Apparatus and Data Collection

To enable data collection, we manufactured a box-shaped object, which can be easily co-manipulated by two subjects (see Figure 2.1). The object weighs 3100 g in total. Its body is made of plexiglass with dimensions of 30 cm × 25 cm × 10 cm and weighs 2538 g. Two aluminum handles, each weighing 231 g, were attached to facing sides of the object. Two ATI-Mini40 force/torque (F/T) sensors, each weighing 50 g, were placed between the handles and the object body to record the forces and torques applied on the side of each subject. These signals were sampled by a USB X Series NI data acquisition system at 1 kHz frequency.

The torques applied by each agent on the object are computed as the cross product of the force measured by the F/T sensor and the position vector defining the point of application (i.e., the sensor) with respect to the object's centre of mass. The computed torque is a vector quantity: $\tau^c = [\tau_x^c, \tau_y^c, \tau_z^c]^T$. It's important to note that due to the placement of the sensors with respect to the users' interaction points (see Figure 2.1), some torques are generated at the handles during a manipulation, which are measured directly by the sensors $\tau^m = [\tau_x^m, \tau_y^m, \tau_z^m]^T$. As a result, we calculate the total torque exerted on each partner's side by summing up these two torque components as:

$$\tau = [\tau_x^c + \tau_x^m , \tau_y^c + \tau_y^m , \tau_z^c + \tau_z^m]^T \tag{2.1}$$

The object's position was tracked by Basler acA 1920-25um USB 3.0 camera using an ArUco marker [49] and the OpenCV library. The marker was placed on the top of the object as shown in Figure 2.1.

2.1.2 Interaction Patterns

Following Madan et al.’s taxonomy of interactive behaviors [25], we defined four interaction patterns to be examined in this study. Two of these are harmonious interaction types with a common intention to start/continue the motion, whereas the remaining two are conflicting interaction types:

(1) Harmonious Translation (HT): The partners agree on translating the object towards a common target configuration.

(2) Conflicting Translation (CT): The dyad faces a conflict as only one of the partners intends to translate the object to the target configuration.

(3) Harmonious Rotation (HR): The partners share the same rotation intention; hence they rotate the object collaboratively.

(4) Conflicting Rotation (CR): The dyad faces a conflict as only one of the partners intends to rotate the object.

2.1.3 Experimental Scenarios

During the experiment, the dyad was instructed to move the object collaboratively in mid-air to visit a set of target configurations, reachable through primitive translation and rotation movements. We artificially created harmonious and conflicting behaviors by providing one of the partners with different target configurations. The role of this partner was always played by the experimenter. This was deliberately done to eliminate implicit role allocations and differences in how people respond to and resolve conflicts. The subjects were briefed that the experimenter will be the supervisor of the task and they should aid him to complete the task in case they felt conflicts.

In return, the subjects’ task sequence was always constant and asked them to:

(1) lift the object up **($\boldsymbol{U}$)**,

(2) rotate it counterclockwise about the *x*-axis **($\boldsymbol{R_x^+}$)**,

(3) translate along the negative *z*-axis into the red target configuration marked on the table **($\boldsymbol{T_z^-}$)**,

(4) translate along the *y*-axis to reach the black target configuration **($\boldsymbol{T_y^+}$)**,

(5) rotate the object clockwise about *x*-axis **($\boldsymbol{R_x^-}$)**, and

(6) put it down **(*D*)**.

In shorter form, the subject's task sequence can be written as $\{U, R_x^+, T_z^-, T_y^+, R_x^-, D\}$. Note that, in this study, all the movement axes refer to the local object coordinates unless stated differently.

The experimenter, on the other hand, was given different target configurations, defining six different scenarios, which are depicted in Figure 2.2. Each of these six scenarios (Sc1-Sc6) aims at isolating more than one of the four specific interaction patterns. The primitive motions that shall be performed by the subject and the experimenter in each scenario are summarized in Table 2.1. The table also indicates the anticipated interaction patterns arising from the interplay between the intended motions of the experimenter and the subject. Figure 2.3 shows a representative experimenter-subject scenario (Sc3) with the expected behaviors.

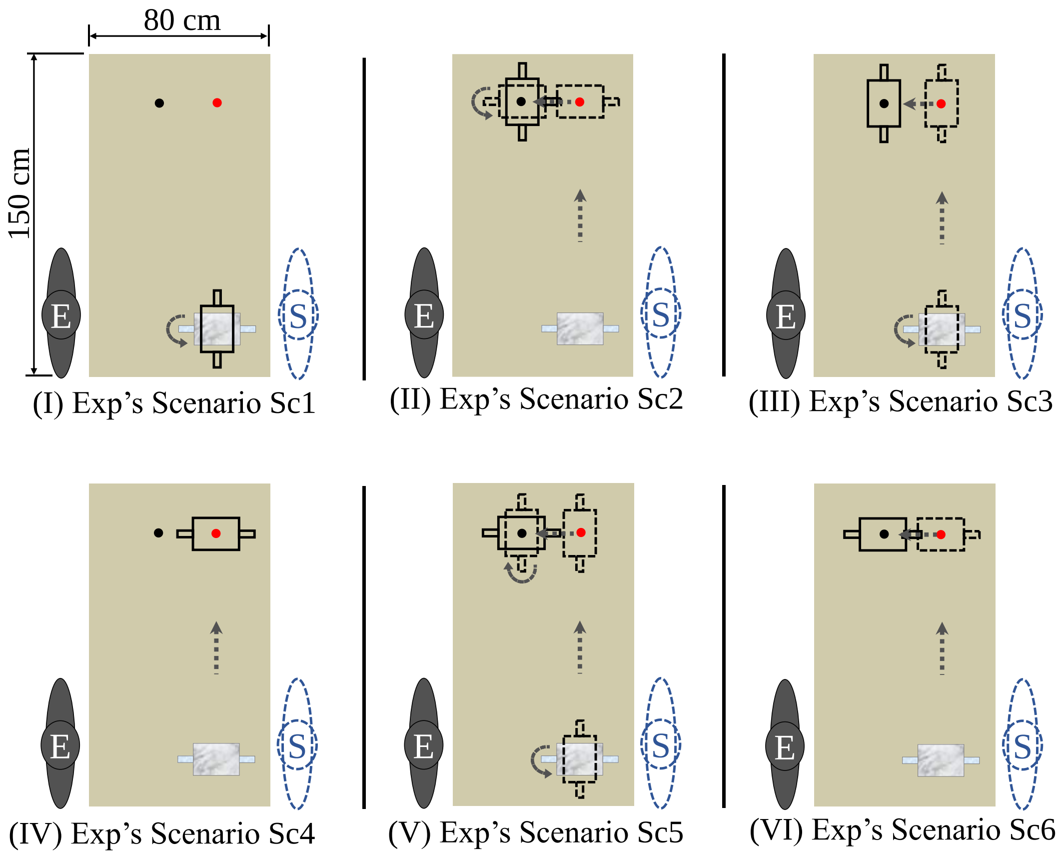

Figure 2.2: (I-VI) Experimenter's (E: Exp) scenarios Sc1-Sc6.

Table 2.1: Primitive motions within the experimental scenarios and the anticipated interaction behaviors. S: Subject, E: Experimenter, Sc1–Sc6: Experimenter's scenarios. *U*: Lift the object up, *D*: Put the object down, *R*: Rotation, *T*: Translation. The superscripts and subscripts for *R* and *T* refer to the direction and axis of the transformation, respectively.

	Primitive Motion (PM) and Expected Behavior (EB)						
S	**PM**	U	R_x^+	T_z^-	T_y^+	R_x^-	D
E: Sc1	**PM**	U	R_x^+	-	D	-	-
	EB		HR	CT	-	-	-
E: Sc2	**PM**	U	-	T_y^+	T_z^+	R_x^+	D
	EB		CR	HT	HT	HR	-
E: Sc3	**PM**	U	R_x^+	T_z^-	T_y^+	-	D
	EB		HR	HT	HT	CR	-
E: Sc4	**PM**	U	-	T_y^+	-	D	-
	EB		CR	HT	CT	-	-
E: Sc5	**PM**	U	R_x^+	T_z^-	T_y^+	R_x^-	D
	EB		HR	HT	HT	HR	-
E: Sc6	**PM**	U	-	T_y^+	T_z^+	-	D
	EB		CR	HT	HT	CR	-

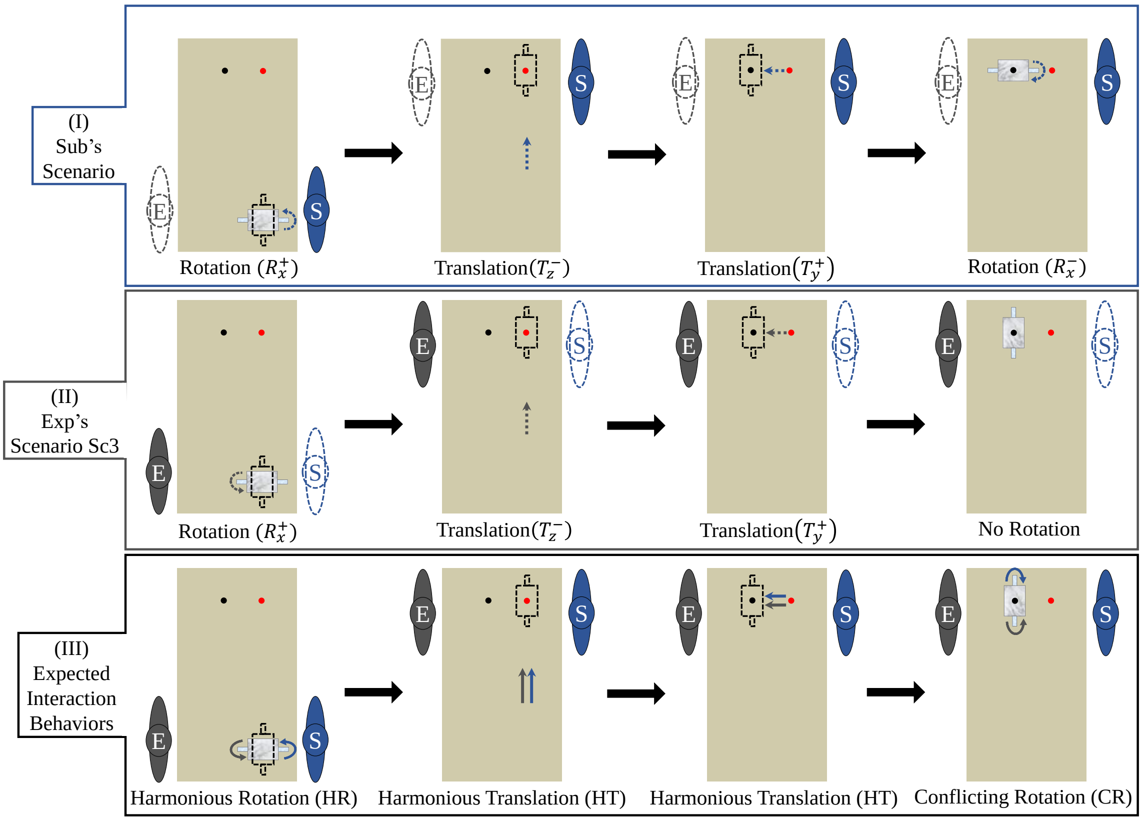

Figure 2.3: (I) Subject's (S: Sub) scenario, consisting of the task sequence $\{U, R_x^+, T_z^-, T_y^+, R_x^-, D\}$, where *U*: lift the object Up, *D*: put the object Down, *R*: Rotation, *T*: Translation. Superscripts and subscripts for *R* and *T* refer to the direction and axis of the transformation, respectively. For simplicity *U* and *D* are omitted from the figure, (II) Individual steps of actions in Experimenter's scenario Sc3: $\{U,\ R_x^+, T_z^-, T_y^+, D\}$ (III) Expected interaction patterns generated due to the interplay between the Subject's and the Experimenter's actions. The red and black dots represent the intermediate and final object configurations as shown to the subject. Dashed arrows represent the partners' intentions, whereas solid arrows represent their actions.

2.1.4 Participants and Protocol

We conducted a study with 12 subjects (8 males and 4 females with an average age of 28.4 ± 7.0 SD) to collect data within a dyadic object transportation task. During the experiment, each subject collaborated with the experimenter to move the object between designated configurations following the patterns in Table 2.1. The experimenter always stood at the same position and acted as the task supervisor. In order to eliminate any visual contact with the experimenter, the subjects wore industrial eye protection glasses which were modified by shading most of the glasses, leaving a small gap at the bottom to observe just the scene.

The subjects started the experiment facing the experimenter, while the object lay on the table. The subjects and the experimenter were instructed to grasp the handle on their side, lift the object up from the table, and move and place it to a target pose by passing through a series of intermediate goal configurations. The dyad performed 12 trials, where scenarios Sc1-Sc6 were executed twice (Table 2.1). The order of the scenarios was randomized but was the same throughout the experiment for all subjects.

In order to achieve synchronization, we implemented two distinctive software beeps: The first beep indicated the partners to grasp the handles gently. The second beep was played after five seconds to indicate the start of the trial, asking the dyad to lift the object up and start the transporting motion.

At the beginning of the experiment, the subjects were briefed about the task, and familiarized themselves with the object. The subjects were given training through experimenting with the task sequence prior to data acquisition. During the training, each subject performed all the scenarios with the experimenter (Sc1-Sc6) once. The subjects were not aware of the experimenter's goal, but they were told that in some trials, the experimenter might have different goal configurations at each step within the task. In such cases, the subjects were asked to collaborate with the experimenter. For instance, if they felt a conflict when trying to rotate the object, they were instructed to stop the rotation and move on to the next task segment along with the experimenter.

2.1.5 Data Segmentation

After data collection, raw haptic data were annotated by the experimenter, who has a good understanding of the interaction behaviors. The annotation was done manually through visual inspection of data based on the expected patterns listed in Table 2.1. Although the primitive motions are designed to elicit anticipated interaction patterns, we further confirmed that these interaction patterns appear in the data. The time-series was first segmented by utilizing the object pose. This was done by observing the object movement along the desired axis based on the designed scenario. For instance, in Sc4, the partners have the same intention to translate the object along y-axis. By inspecting the object movement along this axis, we can see that they successfully translate the object from the start position to the red point, see the pink region in Figure 2.4a. Therefore, we considered this period as a harmonious translation (HT). We used the same procedure to detect the harmonious rotation behaviors through observing the object rotational movement.
However, as the pose information was expected to be static during conflicting behaviors, we used the changes in force and torque commands to segment CT and CR. For instance, the conflicting translation periods were segmented using the changes in forces applied in the direction of conflict. In more details, during this period, the partners applied high forces values in opposite directions to each other along z-axis (see Figure 2.4e) while no considerable movement occurs along that axis, see Figure 2.4b. Likewise, utilizing the changes in the applied torques, the conflicting rotation periods were tightly segmented. For instance, in Sc4, the subject scenario includes a rotation about x-axis, so he/she applies torque about this axis to rotate the object. On the other hand, the experimenter scenario in Sc4 does not include this initial rotation sub-movement. As a result, he would prevent this rotation by applying a torque in the opposite direction to the that applied by the subject to prevent the rotation, see Figures 2.4c and 2.4d. The remaining periods, where no changes are observed in the applied forces/torques, were considered as pauses. After this procedure, each segment was assigned a label, matching one of the four interaction behavior patterns. The haptic data was recorded at a frequency of 1 kHz, and for each time step of our labeled data, the haptic-based features were calculated.

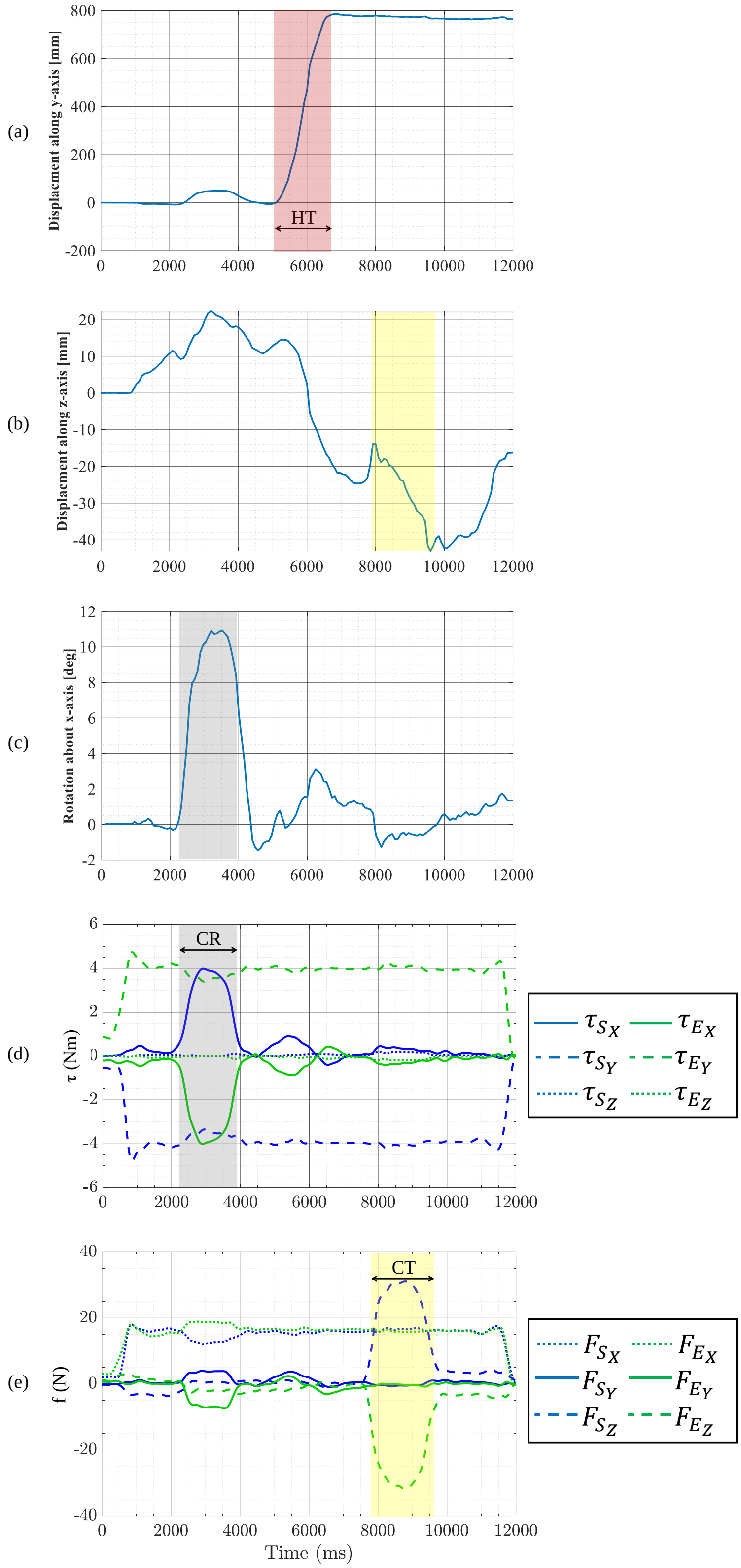

Figure 2.4: Forces, torques, object position, and object orientation generated by a representative dyad under Sc4 for different interaction behaviors.

2.2 Force/Torque Patterns in Interaction Behaviors

This section presents an in-depth investigation of the force/torque patterns encountered in the proposed scenarios. This analysis provides us with essential observations on metrics description and also on feature extraction process, which will be explained in Sections 2.3 and 2.4, respectively.

Figure 2.5 displays the forces and torques generated by a representative dyad in scenarios Sc4 and Sc5. In all plots, subscripts S and E refer to the subject and experimenter, respectively. Please note that all data are reported with respect to the object frame.

Figure 2.5(a) illustrates the forces, F, exerted by each partner. Figures 2.5(b) and 2.5(c) respectively plot the computed torques, τ^c, and the measured torques, τ^m. The total torques applied by each partner (i.e., $\tau = \tau^c + \tau^m$) are depicted in Figure 2.5(d). Finally, Figure 2.5(e) shows the net torques, $\tau_{SUM} = \tau_E + \tau_S$, applied on the object by the dyad.

As shown in Figure 2.5(a), the forces exerted in x-axis have high values and show a similar pattern throughout all four behaviors. This is due to the fact that these forces are used dominantly for gravity compensation. Likewise, the partners exert matching torques about y-axis in opposite directions ($\tau_{SUM_Y} \approx 0$) with a similar pattern throughout all behaviors when lifting the object (see Figures 2.5(d) and 2.5(e)).

During HT behavior (marked pink in Figure 2.5), the partners harmoniously translate the object along a desired axis. For instance, in scenario Sc4 (see Figure 2.2(IV)), the partners harmoniously translate the object along the positive y-axis as they share an intention to translate the object to the red target without rotation. This behavior manifests itself by the partners' applied forces along the direction of motion. In Figure 2.5(a) left panel, both partners apply forces in y-axis to synchronously accelerate the object, and then reverse the direction of the applied forces to decelerate it.

Other examples of HT can be seen in scenario Sc5 (see Figure 2.2(V)). In this scenario, two harmonious translation periods can be observed. In the first one, the partners translate the object cooperatively in the negative z-direction, while in the second period, they translate it along the positive y-direction. In both segments, similar to the behavior observed for HT in scenario Sc4, the partners first accelerate the object

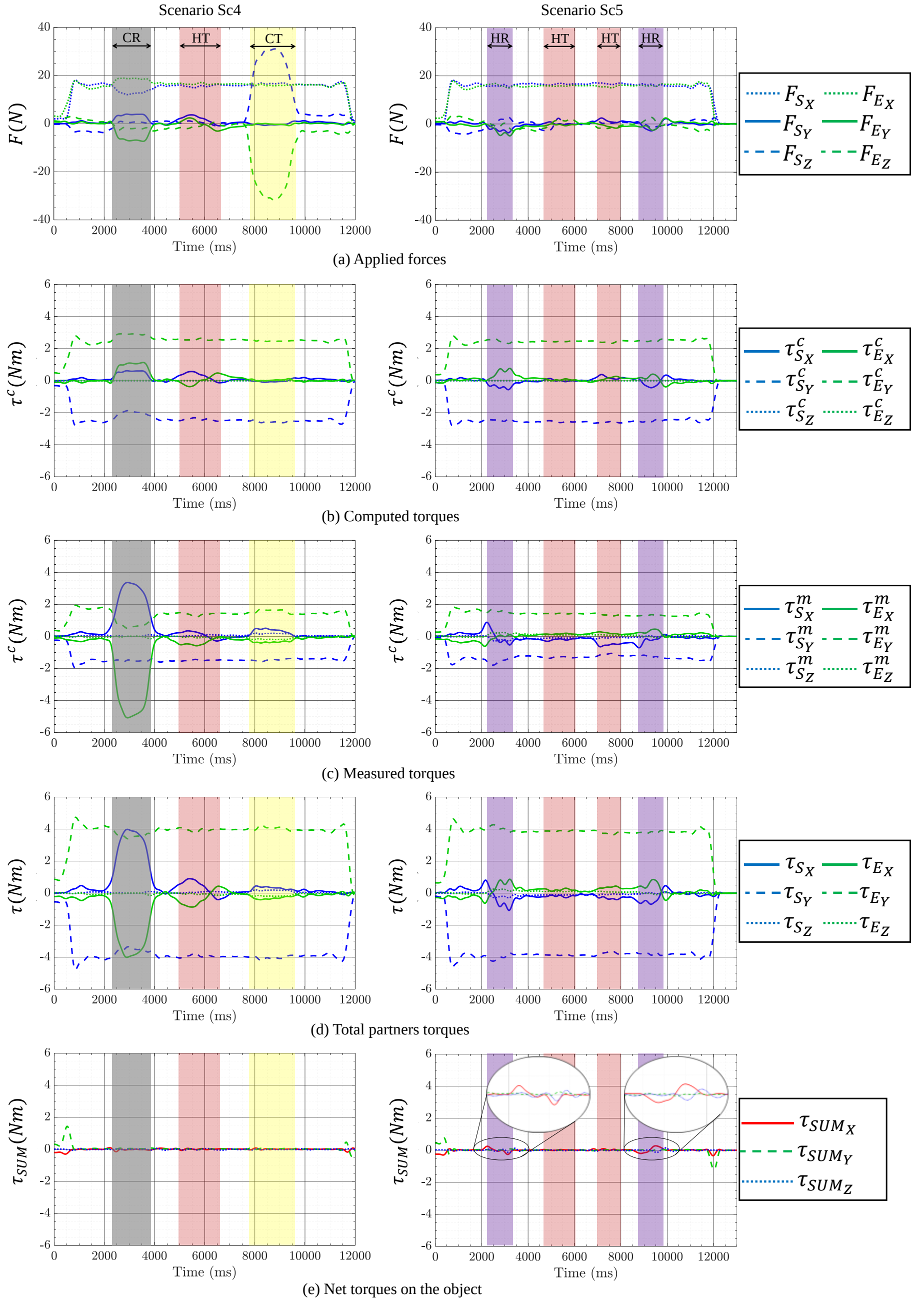

Figure 2.5: Forces and torques generated by a representative dyad under Sc4 and Sc5 for different interaction behaviors. Left and right panels represent the behaviors encountered during Sc4 and Sc5, respectively. CR, HT, CT, and HR refer to conflicting rotation (gray color), harmonious translation (pink color), conflicting translation (yellow color), and harmonious rotation (violet color) periods, respectively. Subscripts S and E refer to the subject and experimenter, respectively. (a) measured (applied) forces F; (b) computed torques τ^c; (c) measured torques τ^m; (d) total applied torques by each partner τ; (e) net torques applied on the object by the dyad, $\tau_{SUM} = \tau_E + \tau_S$.

by applying forces in the desired direction of motion, then reverse the force direction to decelerate it (see Figure 2.5(a) right panel).

However, it is worth to mention that in some HT periods, when one partner applies force in the direction of movement to accelerate the object, due to the speed mismatch between the partners, this force creates a reaction force on the second partner's handle. Since the second partner has the same intention to translate the object, he/she tries to contribute in the translation by compensating the reaction force to provide the relevant compliance to his/her partner.

In CT behavior (marked yellow in Figure 2.5), the partners disagree on the intended translation motion. This behavior is generated in scenario Sc4, where the subject and the experimenter have different goals, i.e., the experimenter aims at reaching the red point as shown in Figure 2.2(IV) and terminates the task, whereas the subject's initial goal is to proceed to the black point (see Figure 2.3(I)). This disparity between the goals creates a conflict, which is observable through investigating the forces along the z-axis. As shown in Figure 2.5(a) left panel, the subject wants to translate the object after reaching the red dot; hence he/she applies a force along the z-direction. However, the experimenter aims to stay on the red point without incurring any further translation. As a result, he conflicts with subject's translation intention by applying a force in the opposing direction, so that no translation occurs.

In CR behavior (marked grey in Figure 2.5), the partners disagree on the intended rotation of the object. In this scenario, the subject aims to rotate the object at the beginning of the task (see Figure 2.3(I)). However, as shown in Figure 2.2(IV), the experimenter's scenario (i.e., scenario Sc4) does not involve that initial rotation. Therefore, the experimenter conflicts the subject and tries to prevent him/her from rotating the object. In effect, both partners apply forces along the y-axis; however, since their intentions are different, these forces are expected to be in the same direction to generate opposing torques, which should cancel out as long as the conflict is not resolved. However, investigating Figures 2.5(a) and 2.5(b) left panel, we observe that the exerted forces on partners' sides along y-axis are in opposite directions, creating torques in the same direction (i.e., the computed torques τ^c around x-axis). Nevertheless, inspecting the object pose reveals that the experimenter succeeded in preventing the object rotation. This can be clarified by observing the torques measured by the sensors on the handles, τ^m, which indicate the dominant opposition in torques about x-axis (see Figure 2.5(c) left panel). Summing up τ^c and τ^m to compute the applied torques on each partner's handel, τ, reveals that opposing torques of comparable magnitudes are exerted on the partners' handels about x-axis. This results in approximately zero net torque on the object about the x-axis, τ_{sum_x}, as shown in Figure 2.5(e) left panel, causing no apparent rotation in the final motion.

Finally, in HR behavior (marked violet in Figure 2.5), the partners share the intention to rotate the object in the same direction. Consequently, they work cooperatively to rotate the object. This is expected to be realized by applying torques in the same direction about the axis of rotation. However, we see that the torques applied by partners about x-axis are in opposite directions as illustrated in Figures 2.5(b)-(d) right panel. An explanation for this ambiguity is the out of synchronization of partners since each of them has his/her own reaction time to start the movement. In our experiments, we observed that it is hard for the dyad to synchronize their movement when rotating the object. In reality, the rotation is initiated by one partner, who applies a torque in the direction of rotation. This torque, due to the difference in partners' reaction time [20], produces a reaction torque on the second partner's handle. Since the second partner shares the same intention to rotate the object cooperatively, he/she tries to contribute to the rotation by compensating the reaction torque and adjusts the torque to provide the relevant compliance to his/her partner. This observation is consistent with Stefanov et al.'s observation in [19] about executor and conductor roles in dyadic operation. Figure 2.5(d) right panel illustrates τ_S and τ_E. The torque exerted by one partner about x-axis is higher and in the opposite direction than the torque exerted by the second partner. As a result, some net torque is applied on the object by the dyad about the x-axis (i.e., τ_{SUM_X}), which generates the resulting rotation of the object (see Figure 2.5(e) right panel).

HR is encountered twice in scenario Sc5 (see Figure 2.2(V)). The first rotation is counterclockwise, which requires the partners to apply a positive net torque about x-axis to accelerate the object (i.e., $+\tau_{SUM_X}$). We observed that after starting the rotation, the dyad reversed the direction of the net torque to decelerate the object. In the second occurrence of HR, the direction of rotation is clockwise. To accomplish this rotation, the partners applied a negative net torque about x-axis (i.e., $-\tau_{SUM_X}$) to accelerate the object and then reversed the net torque direction to decelerate it, as shown in Figure 2.5(e) right panel.

The conclusions we reach from these observations are as follows:

1) Due to the physical setup, we verified that the applied torques on the object shall be calculated using the summation of the computed and the measured torques.

2) Each interaction behavior generates unique and complex force or torque patterns. due to the complexity of the signals, a machine learning approach is needed to differentiate the interaction behaviors.

3) Using forces or torques in isolation would be inadequate to classify the behaviors (see Section 2.5.1 for more details). Hence, the integration of force and torque information is essential to describe the motion patterns in each of the four interaction behaviors.

4) Due to the nature of the manipulation task, some force and torque variables (e.g., those used for gravity compensation) may have significantly higher values, without being informative for classification. Hence, a plane-based analysis is desirable.

2.3 Haptic-Related Metrics for Dyadic Collaboration

Our hypothesis in this study is that haptic information plays an essential role for the classification of interaction patterns. In [25] [26], it has been shown that the raw haptic data were insufficient to achieve good classification rates and the kinematic information of manipulated object was needed. However, this requires object tracking, which can typically be achieved through external sensing. In this study, we eliminate the need for object pose by designing a set of haptics-related features to train the behavior classification model. These features are computed based on the metrics proposed by Noohi and Žefran to quantify the collaboration quality on a 1-DoF task [16]. In this section, we present these metrics and provide details on how we modified them to handle 6-DoF motion.

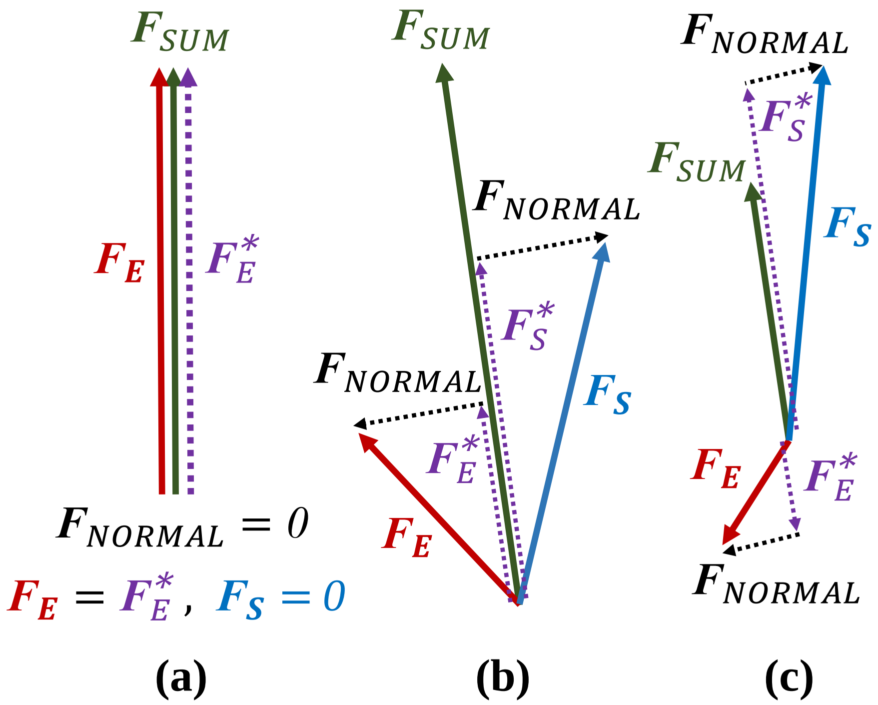

Figure 2.6: Force decomposition (adopted from Noohi and Žefran [16]). F_E, F_S, and F_{SUM} are the forces applied by the experimenter and subject and their summation, respectively. F_E^* and F_S^* are the effective forces for the experimenter and subject, respectively. F_{NORMAL} is the normal force.

In order to put the following equations in context, assume the scenario, where the experimenter (E) and the subject (S) exert forces F_E and F_S on an object. The resultant net force acting on the object is then computed as $F_{SUM} = F_E + F_S$. We decompose the force applied by each partner into two components: an effective force component that is in the direction of F_{sSUM} and contributes to the task, and a normal component, that is canceled out during the interaction by the forces applied by the other partner in the normal direction. The effective forces F_E^* and F_S^*, applied on the object by the experimenter and the subject, are computed respectively as the projection of F_E and F_S on the net force, F_{SUM}, as shown in Figure 2.6. Since the effective forces contribute to the net force in variable degrees, they can be written as:

$$F_E^*(t) = \alpha F_{SUM}(t) \tag{2.2}$$

$$F_S^*(t) = \beta F_{SUM}(t) \tag{2.3}$$

where $\alpha + \beta = 1$, and t stands for the current time step.

The force cooperation index δ represents the extent to which the partners help each other and can be computed as:

$$\delta = 1/2 - \alpha \tag{2.4}$$

where α is defined in eq. (2.2). $\delta = 0$ indicates that each partner carries out half of the voluntary effort during the task. When $|\delta(t)| \leq 0.5$, partners work in a collaborative mode: either both partners exert forces in the direction of the net force as seen in Figure 2.6(b), or one partner is passive as seen in Figure 2.6(a). In contrast, when one partner's force is in the opposite direction to the net force, as in Figure 2.6(c), the partners work in a non-collaborative mode with $|\delta(t)| > 0.5$.

In the rest of this section, we summarize the force-related metrics, which are used as features for behavior classification.

- ***Individual efficiency:*** This assesses to what extent a partner's exerted force contributes to his/her effective force:

$$M_{E_K}^F(t) = \frac{\|F_K^*(t)\|}{\|F_K(t)\|} \tag{2.5}$$

where k refers to the experimenter (E) or the subject (S) and
$0 \leq M_{E_K}^F(t) \leq 1$. The individual efficiency is maximized when $M_{E_K}^F = 1$.

- ***Team efficiency:*** The efficiency of the dyad as a team is defined as the ratio of the magnitude of the net force to the sum of the magnitudes of individual forces exerted by partners:

$$M_{TE}^F(t) = \frac{\|F_{SUM}(t)\|}{\|F_E(t)\| + \|F_S(t)\|} \tag{2.6}$$

where $0 \leq M_{TE}^{F}(t) \leq 1$. When M_{TE}^{F}(t) = 1, no effort is wasted, i.e., the individual forces and the effective forces are the same and $\|F_{NORMAL}(t)\|$= 0; hence team efficiency is maximum. When M_{TE}^{F}(t) = 0, the partners cancel each other' forces, i.e., $\|F_{SUM}(t)\|$= 0; hence team efficiency is minimum.

- ***Negotiation efficiency:*** The efficiency of the negotiation process represents the extent of disagreement between the partners at a given time during the task:

$$M_{NE}^{F}(t) = \frac{\|F_{SUM}(t)\|}{\|F_{E}^{*}(t)\| + \|F_{S}^{*}(t)\|} \tag{2.7}$$

where $0 \leq M_{NE}^{F}(t) \leq 1$. Note that whenever the interaction is in a collaborative mode, $|\delta(t)| \leq 0.5$, the negotiation efficiency is maximum, such that M_{NE}^{F}(t) = 1. Otherwise, M_{NE}^{F}(t) < 1.

- ***Similarity of forces:*** This represents the similarity between the effective forces exerted individually by partners:

$$M_{S}^{F}(t) = 1 - \left| \frac{\|F_{E}^{*}(t)\| - \|F_{S}^{*}(t)\|}{\|F_{SUM}(t)\|} \right| \tag{2.8}$$

where $0 \leq M_{S}^{F}(t) \leq 1$. When the partners work in collaborative mode ($|\delta(t)| \leq 0.5$), we have $0 \leq M_{S}^{F}(t) \leq 1$. Maximum similarity, $M_{S}^{F}(t) = 1$, means that both partners exert exactly half of the voluntary effort. When $M_{S}^{F}(t) = 0$, the partners are in non-collaborative mode ($|\delta(t)| > 0.5$).

As discussed in Section 2.2, some interaction behaviors share very similar force patterns, and can be distinguished only through investigating the torque patterns. Therefore, we extend the above definitions to describe torque-related information as an effort to extract more comprehensive and informative features and improve the classification results. The torque metrics are computed in a very similar fashion to how it's done for the force metrics. Table 2.2 provides the relevant formulations for the wrench metrics, combining the force and torque-based metrics designed and used in this study.

Table 2.2: Wrench-based metrics.

Metric	**Formula**
Individual force efficiencies	$M_{E_K}^{F}(t) = \frac{\|F_K^*(t)\|}{\|F_K(t)\|}$
Team force efficiency	$M_{TE}^{F}(t) = \frac{\|F_{SUM}(t)\|}{\|F_E(t)\| + \|F_S(t)\|}$
Negotiation force efficiency	$M_{NE}^{F}(t) = \frac{\|F_{SUM}(t)\|}{\|F_E^*(t)\| + \|F_S^*(t)\|}$
Similarity of forces	$M_S^F(t) = 1 - \left\vert\frac{\|F_E^*(t)\| - \|F_S^*(t)\|}{\|F_{SUM}(t)\|}\right\vert$
Individual torque efficiencies	$M_{E_K}^{\tau}(t) = \frac{\|\tau_K^*(t)\|}{\|\tau_K(t)\|}$
Team torque efficiency	$M_{TE}^{\tau}(t) = \frac{\|\tau_{SUM}(t)\|}{\|\tau_E(t)\| + \|\tau_S(t)\|}$
Negotiation torque efficiency	$M_{NE}^{\tau}(t) = \frac{\|\tau_{SUM}(t)\|}{\|\tau_E^*(t)\| + \|\tau_S^*(t)\|}$
Similarity of torques	$M_S^{\tau}(t) = 1 - \left\vert\frac{\|\tau_E^*(t)\| - \|\tau_S^*(t)\|}{\|\tau_{SUM}(t)\|}\right\vert$

2.4 *Feature Extraction and Classifier Design*

After performing the experiment, the raw data were processed to create a labelled dataset of force and torque-based metrics as features, consisting of our data points as instances and the metrics as features. The data were labelled based on the segmentation explained in Section 2.1.5.

2.4.1 Feature Extraction

As discussed in Section 2.2, the object movement that is relevant to our interaction behaviors are mainly in the *y-z* plane for the current task. However, as we are targeting classification for unconstrained transportation, it's interesting to investigate interactions between task DoFs. In this regard, it is possible to extract features from the data using the net forces/torques acting on the object in 3D space; or alternatively, one can analyze the task in different movement planes and extract features for each of these planes. We hypothesized that the latter approach would be more informative for classification as it can extract the characteristics, we observed for each behavior better. In particular, as our observations in Section 2.2 indicate that large lifting forces in x-axis and torques around y-axis, which are not directly pertinent to the interaction patterns, could dominate subtle force and torque patterns which could be relevant to the interaction dynamics. Hence, we hypothesize that in contrast to a space-based feature extraction method, extracting features on separate planes can eliminate such difficulties.

In order to compute plane-based features, we focused on 3 principal orthogonal movement planes in Cartesian space, i.e., *x-y*, *x-z*, and *y-z*. Let's assume A refers to a specific plane $A \in \{x\text{-}y, x\text{-}z, y\text{-}z\}$. The forces exerted by the experimenter, F_{E_A}, and the subject, F_{S_A}, on these planes are computed using a projection operation. The net force applied on the object by the partners on plane A is computed as $F_{SUM_A} = F_{E_A} + F_{S_A}$. The effective forces applied by the dyad, $F^*_{E_A}$ and $F^*_{S_A}$, are computed as the projection of F_{E_A} and F_{S_A} on F_{SUM_A} in 2D as explained in Section 2.3.

The torque decomposition is done in a very similar fashion to forces. In the plane-based analysis, we consider the torques perpendicular to the plane A. For each partner, these torques are generated by summing up the measured torques about the axis perpendicular to the plane A and the torques caused by the applied forces in plane A (i.e., the computed toques). These generated torques are denoted by τ_{E_A} and τ_{S_A} for the experimenter and the subject, respectively. Accordingly, the net torque applied by the partners on the object perpendicular to the plane A is computed as $\tau_{SUM_A} = \tau_{E_A} + \tau_{S_A}$. Since τ_{E_A} and τ_{S_A} are in the same direction of τ_{SUM_A}, they are considered as the effective torques perpendicular to the plane A of the experimenter and the subject respectively (i.e., $\tau^*_{E_A} = \tau_{E_A}$ and $\tau^*_{S_A} = \tau_{S_A}$).

Using these two approaches, we evaluate two different ways of feature extraction from raw data. This results with two feature sets of differing sizes as summarized in Table 2.3:

1) **Space-Based Features:** Wrench-related metrics are calculated by considering the force/torque decomposition in 3D. This process results with 10 metrics (i.e., 5 force-related and 5 torque-related) as explained in Section 2.3.
2) **Plane-Based Features:** We perform force/torque decomposition separately for each principal movement plane, *x-y*, *x-z*, and *y-z*. That results with 30 metrics (i.e., 5 force-related metrics × 3 planes and 5 torque-related metrics × 3 planes).

Table 2.3: Wrench-based features

Features	Description	No. of Features	
		Space-Based	Plane-Based
$M^F_{E_K}$, $M^\tau_{E_K}$	Individual efficiencies	1×4	3×4
M^F_{TE}, M^τ_{TE}	Team efficiency	1×2	3×2
M^F_{NE}, M^τ_{NE}	Negotiation efficiency	1×2	3×2
M^F_S, M^τ_S	Similarity	1×2	3×2
Total		10	30

2.4.2 Classifier Design

We used a random forest classifier to distinguish between the aforementioned interaction patterns. Random forest is an ensemble learning algorithm, which combines multiple decision trees, i.e., a forest. The algorithm works by learning decision trees on different subsamples from the dataset and uses averaging to select the correct class for multi-class classification given a multitude of decision tree results. In this study, we used the Python Scikit-Learn implementation of the algorithm [50]. The number of trees in the random forest was set to 100, the maximum depth of the trees was unconstrained (i.e., the nodes were expanded until all leaves are single samples), and the quality of a split is measured through information gain.

In our experiments, we investigated the use of different feature sets. To evaluate which feature set is superior to others, we trained a separate classifier for each feature type. To verify the classification performance and to avoid overfitting, the dataset (consisting of the features and corresponding behavior labels) was split into two distinct parts as the training and test sets. The splitting was done by selecting data coming from 8 trials from all the subjects as the training set, and the remaining 4 trials' data as the test set. This procedure sets aside the test set to be reserved for verifying the model. The training set is used to learn the classification model. Once training is done, the test set is used to assess the performance of the trained classifier.

The classifier performance was evaluated using the correct classification rate (accuracy), normalized confusion matrix, and the balanced error rate (BER).

Once we assessed the overall success of each feature set, we selected the top achiever, and investigated how the corresponding classifier performs when the test data comes from a subject, who wasn't included in the training set. For this purpose, we conducted leave-one-out (L1O) cross validation, where we used the data from 11 subjects as the training set and assessed the performance of the trained classifier using the 12th subject's data as the test set. The procedure was repeated looping through all subjects, so that each subject's data was isolated once over the analysis. In addition, we performed feature selection on the top achiever to analyze which subset of features optimize the classification accuracy.

2.5 Results and Discussion

In this section, we first discuss the classification results for isolated force and torque-based feature sets. Afterwards, we present the results achieved by combining force and torque-based features to create a wrench-based feature set. Finally, we perform feature selection and discuss the optimal feature set, which is most informative for the task at hand.

2.5.1 Classification with Isolated Force and Torque-based Feature Sets

In Section 2.2, we observed that while the force information can sufficiently describe the motion in some behaviors (e.g., *HT*), torque information is more informative in describing the motion in other behaviors (e.g., *HR*). Accordingly, we argued that relying on neither the force nor torque features alone would be sufficient.

In order to demonstrate our argument, we trained 4 classification models using the data coming from 8 trials from all subjects and then tested them with the remaining 4 trials' data. In creating the feature sets, we considered using either the force data alone, or the torque data. Moreover, two decomposition approaches explained in Section 2.4.1, namely, the space-based and plane-based methods, are adopted. This resulted with four different feature sets (see Table 2.3):

- **FSB Force Space-Based Feature Set:** Features are extracted using the 5 force-related metrics computed using the space-based decomposition approach.
- **FPB Force Plane-Based Feature Set:** Features are extracted using the 15 force-related metrics computed using plane-based decomposition approach.
- **TSB Torque Space-Based Feature Set:** Features are extracted using the 5 torque-related metrics computed using space-based decomposition approach.
- **TPB Torque Plane-Based Feature Set:** Features are extracted using the 15 torque-related metrics computed using plane-based decomposition approach.

The classifiers trained with FSB and FPB respectively achieve classification accuracies of 60.68% and 68.06% with BERs of 0.34 and 0.27.

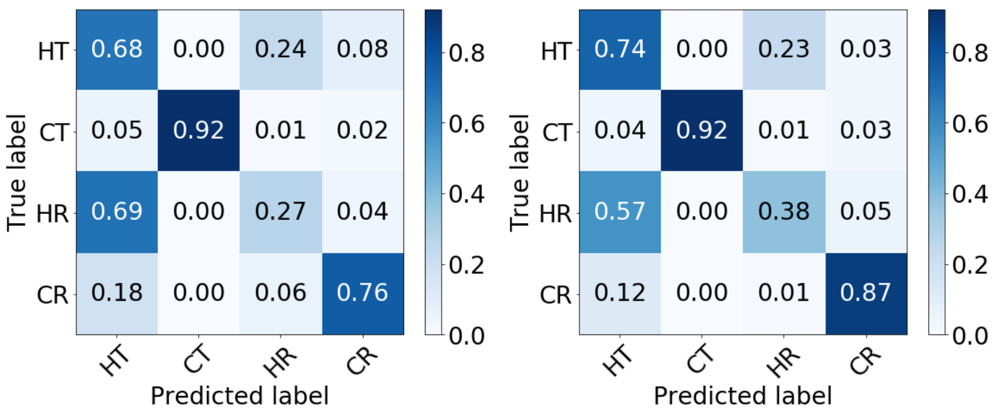

(a) (b)

Figure 2.7: Confusion matrices for a) classifier trained with FSB feature set and b) classifier trained with FPB feature set. HT, CT, HR, and CR denote harmonious translation, conflicting translation, harmonious rotation, and conflicting rotation, respectively.

Figure 2.7 shows the confusion matrices for each feature set. As seen here, both classifiers are particularly unsuccessful distinguishing between HR and HT patterns, and score as poor as random guessing (i.e., 25%) when trained with FSB.

Using the plane-based features improves classification rates slightly, however, does not manage to solve the confusion between HR and HT.

In contrast, the classifiers trained with TSB and TPB achieve classification accuracies of 47.92% and 71.37% and BERs of 0.61 and 0.34, respectively. The confusion matrices are shown in Figure 2.8.

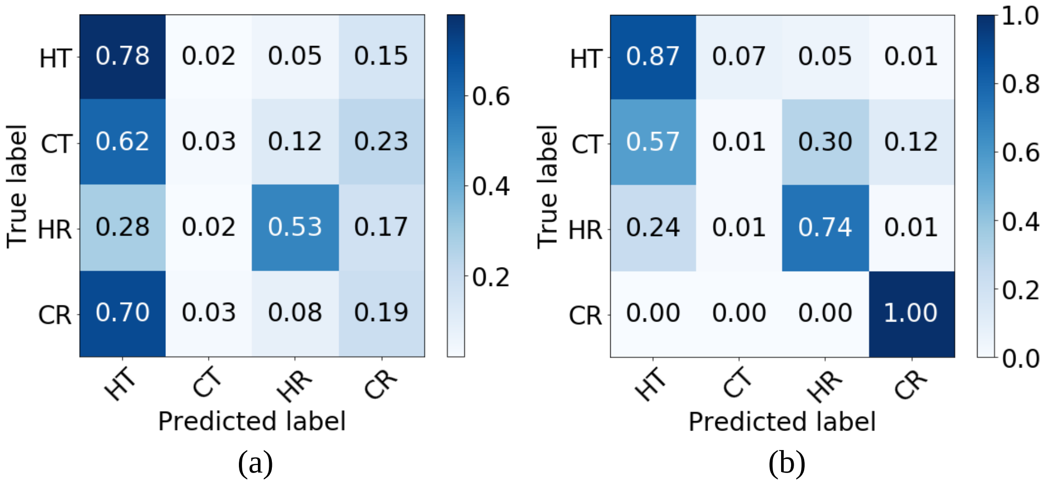

Figure 2.8: Confusion matrices for a) classifier trained with TSB feature set and b) classifier trained with TPB feature set. HT, CT, HR, and CR denote harmonious translation, conflicting translation, harmonious rotation, and conflicting rotation, respectively.

Evidently, the torque-based features perform very poorly. Using the space-based decomposition, the classifier fails to distinguish CT, CR and HR. Adopting the plane-based approach drastically improves the classification of CR. However, neither feature sets (i.e., TSB and TPB) can improve the classification rate of CT.

These results show that the classifiers trained with the plane-based features achieve higher accuracies in comparison to those trained with features extracted using the space-based approach. However, these features cannot eliminate the confusion between HT vs HR using only force-related features and have failed in classifying CT correctly with the torque-related feature sets.

2.5.2 Classification with Wrench-based Feature Set

Since using either force or torque data alone was inadequate to generate feature sets capable of distinguishing between the interaction behaviors, we combined these to create a wrench-based features. In similar fashion to the previous section, we created two feature sets:

- **WSB** Wrench Space-Based Feature Set: Features are extracted using the 10 force/torque-related metrics computed using space-based decomposition approach (i.e., 5 force-related metrics and 5 torque-related metrics).
- **WPB** Wrench Plane-Based Feature Set: Features are extracted using the 30 force/torque-related metrics computed using plane-based decomposition approach (i.e., 15 force-related metrics and 15 torque-related metrics).

Accordingly, two classifiers were trained with data coming from 8 trials considering all the subjects' data. After training the classifiers, we tested them with the remaining 4 trials' data. The results indicate that WSB classifier achieves an accuracy of 78.59% and BER of 0.20, whereas the WPB classifier achieves an accuracy of 91.02% and BER of 0.08. The confusion matrices for the both classifiers are shown in Figure 2.9.

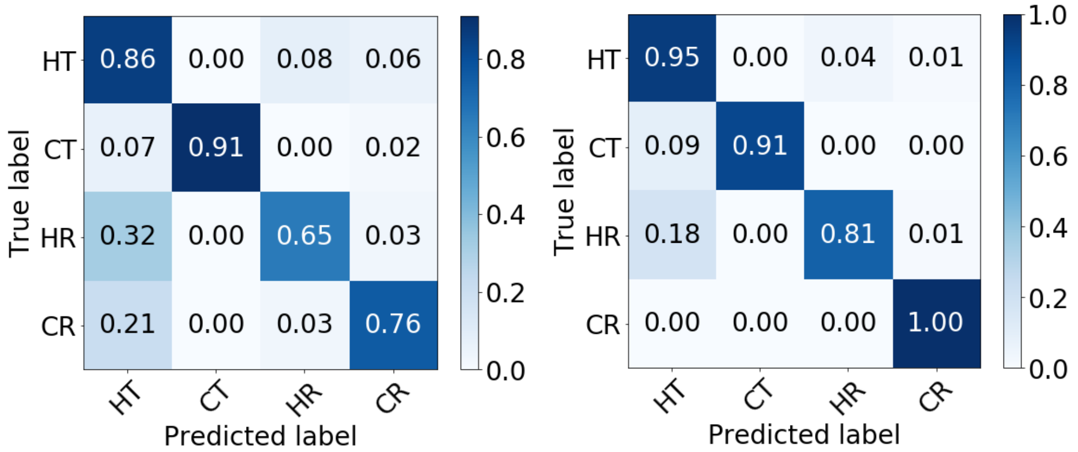

(a) (b)

Figure 2.9: Confusion matrices for a) classifier trained with WSB feature set and b) classifier trained with WPB feature set. HT, CT, HR, and CR denote harmonious translation, conflicting translation, harmonious rotation, and conflicting rotation, respectively.

The results show that utilizing the wrenches (i.e., combining force and torque information) makes our feature set more robust, and leads to a significant increase in classification accuracy. Although both classifiers can successfully separate all behaviors, the WPB feature set achieves better classification rates. This means that the features extracted by the plane-based force/torque decomposition are more informative than those extracted by the space-based technique. To be fairer, the plane-based force/torque decomposition resulted with more features number than the space-based technique (i.e., 30 features vs 10 features), this might be also a reason of getting a better classification result when the plane-based force/torque decomposition technique is used.

We used some other machine learning algorithms such as support vector machine and ANN. Figure 2.10 shows the confusion matrix for SVM classifier trained with WSP feature set.

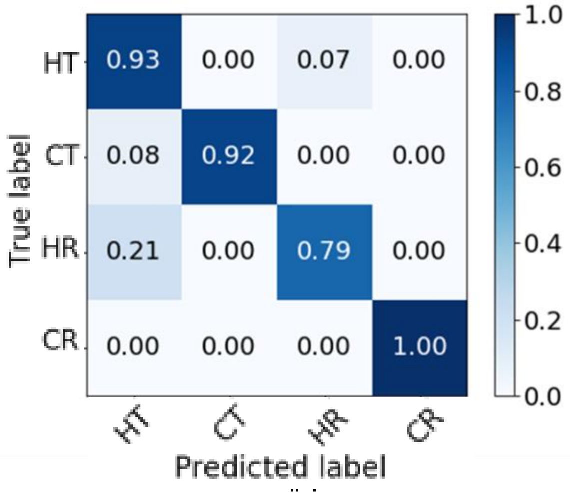

Figure 2.10: Confusion matrix for SVM classifier trained with WPB feature set. HT, CT, HR, and CR denote harmonious translation, conflicting translation, harmonious rotation, and conflicting rotation, respectively.

As mentioned in Section 2.4.2, L1O cross-validation was used to investigate how the best achieving feature set performs when the data comes from a new subject. We tested this procedure with the WPB feature set, and achieved an average accuracy of 88.69% and average BER of 0.094. Figure 2.11 shows the average confusion matrix for this classifier. As can be seen, the classification rates are consistent with the original protocol, and demonstrates good generalization for different users.

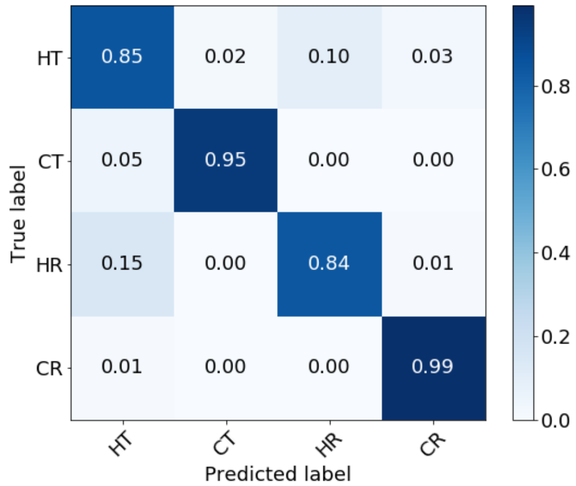

Figure 2.11: Confusion matrix for classifier trained with WPB feature set utilizing L1O protocol. HT, CT, HR, and CR denote harmonious translation, conflicting translation, harmonious rotation, and conflicting rotation, respectively.

2.5.3 The Optimal Feature Set Selection

To conclude our analyses, we performed feature selection to discover the optimal feature set to train the classification model. We used the mean decrease impurity (MDI) method (sometimes called gini importance) for feature ranking [48]. MDI represents importance regarding how many times a feature is used to split a node, weighted by the number of samples in the node. The decrease in node impurity is summed for each feature and averaged across all trees in the forest.

Table 2.4 presents the feature ranking provided by MDI. In order to select the most relevant subset of features, we perform forward selection: Starting with an empty subset, we iteratively add the features to the model, based on the feature importance as given by

MDI. Then, for each feature subset, we compute the performance of the model. Figure 2.12 shows the output of this process.

The optimal feature set that maximizes classification accuracy consists of the first 25 features in Table 2.4 with a classification accuracy of 91.25% and a BER of 0.07.

However, as can be seen in Figure 2.12, the accuracy is almost constant after including the first 13 features (89.78% accuracy, 0.09 BER), and reaches a good level with only 5 features (85.66% accuracy, 0.12 BER). We observe a large drop in classification accuracy when the feature subset is limited to the first 4 features (69.62% accuracy, 0.35 BER).

Figure 2.13 shows the confusion matrices for the classifiers trained with these feature subsets, consisting of 25, 13, 5 and 4 features. Although the classifier trained with an optimal feature set consisting of 25 features achieves the higher accuracy with a minimum classification rate of 82% for HR, the classifiers trained with 13 and 5 features also achieve good accuracies with a minimum classification rate of 70% for HR. On the other hand, when we train the classifier with only the first 4 features, the overall accuracy drops to 69% with strong misclassification for the CT behavior. Observing Table 2.4 reveals that this optimal feature set does not contain any force information. This indicates the necessity of force information to describe the translation behaviors (i.e., HT and CT) as we have observed in Section 2.2.

Table 2.4 indicates the importance of individual torque efficiencies about y-axis, $M_{E_S}^{\tau}(y)$ and $M_{E_E}^{\tau}(y)$, as they come in the 1st and the 3rd in ranks, respectively. Our observations in Section 2.2 indicate that the applied torques about y-axis have a similar pattern with high values across all behaviors. We can see in Figure 2.5 that the individual torques about the y-axis drop slightly in magnitude under CR. This is coupled by a dramatic change in the applied torques around the x-axis. The efficiency is computed as the ratio of individual torques about y-axis to the norm of the total applied torque by that partner in 3D. Hence, $M_{E_S}^{\tau}(y)$ and $M_{E_E}^{\tau}(y)$ capture important information to distinguish CR from other behaviors.

Table 2.4: Feature ranking provided by MDI

Rank	Metric	Importance (%)	Rank	Metric	Importance (%)
1	$M^{\tau}_{E_S}(y)$	12.39	**16**	$M^{F}_{NE}(yz)$	2.05
2	$M^{\tau}_{E_S}(x)$	10.90	**17**	$M^{F}_{E_E}(yz)$	1.89
3	$M^{\tau}_{E_E}(y)$	9.80	**18**	$M^{F}_{E_S}(yz)$	1.71
4	$M^{\tau}_{TE}(x)$	8.72	**19**	$M^{F}_{S}(xy)$	1.63
5	$M^{F}_{E_S}(xy)$	7.47	**20**	$M^{F}_{S}(xz)$	1.50
6	$M^{\tau}_{E_E}(x)$	6.78	**21**	$M^{F}_{TE}(yz)$	1.32
7	$M^{F}_{E_E}(xz)$	4.17	**22**	$M^{\tau}_{NE}(z)$	0.63
8	$M^{F}_{E_S}(xz)$	4.08	**23**	$M^{F}_{S}(yz)$	0.54
9	$M^{F}_{TE}(xy)$	4.05	**24**	$M^{\tau}_{NE}(y)$	0.41
10	$M^{F}_{E_E}(xy)$	4.04	**25**	$M^{\tau}_{TE}(y)$	0.39
11	$M^{\tau}_{NE}(x)$	3.92	**26**	$M^{\tau}_{S}(x)$	0.34
12	$M^{F}_{TE}(xz)$	3.19	**27**	$M^{\tau}_{S}(z)$	0.11
13	$M^{\tau}_{E_E}(z)$	2.94	**28**	$M^{F}_{NE}(xy)$	0
14	$M^{\tau}_{E_S}(z)$	2.58	**29**	$M^{F}_{NE}(xz)$	0
15	$M^{\tau}_{TE}(z)$	2.31	**30**	$M^{\tau}_{S}(y)$	0

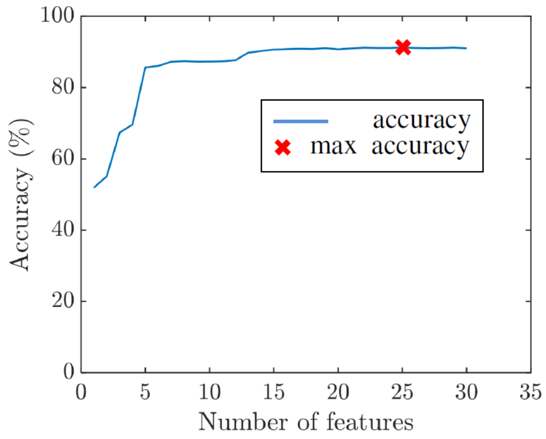

Figure 2.12: Classification accuracy vs number of features added to the model incrementally using MDI ranking.

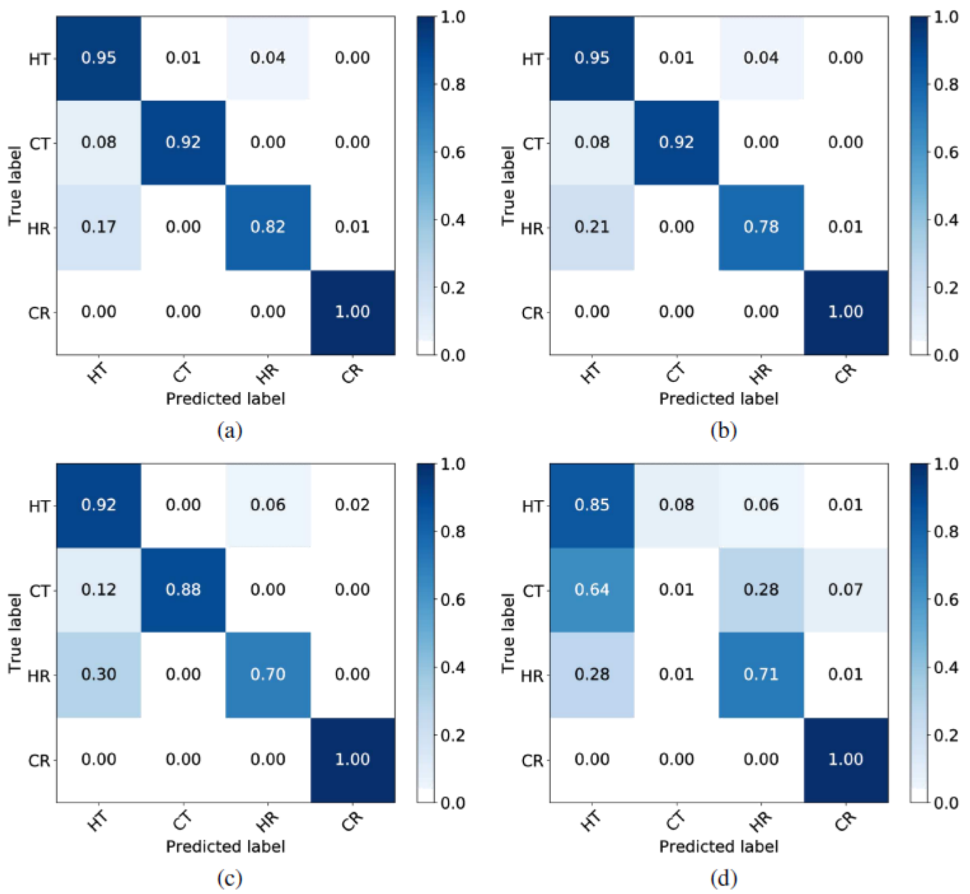

Figure 2.13: Confusion matrices for classifier trained with the optimal WPB feature set containing: (a) 25 features, (b) 13 features, (c) 5 features, and (d) 4 features.

In addition, $M^{\tau}_{E_S}(x)$ and $M^{\tau}_{E_E}(x)$ find high places (i.e., 2nd and 6th) in the feature importance ranking. This is due to the prevalence of the torques around x-axis as shown in Figure 2.5. Thus, they are informative for differentiating CR.

Team torque efficiency about x-axis, $M^{\tau}_{TE}(x)$, is the 4th important feature. It represents the ratio of the net torque applied on the object about x-axis divided by the norm of the total applied torque by the partners in 3D. Considering that there is no explicit rotation in HT, CT, and CR, the numerator for this metric (i.e., τ_{SUM_X}) has always a small value (i.e., near zero, see Figure 2.5(e)). On the other hand, in HR, the numerator, τ_{SUM_X}, has relatively a high value, which helps in rotating the object (see Figure 2.5(e)). Due to this, $M^{\tau}_{TE}(x)$ is informative to differentiate HR than other behaviors. As a result, the first four important features in Table 2.4 can differentiate HR and CR from HT and CT (see Figure 2.13(d)).

In the 5th, 9th, and 10th importance ranks (see Table 2.4), we have the individual and team force efficiencies in *x*-*y* plane $M^{F}_{E_S}(xy)$, $M^{F}_{TE}(xy)$, and $M^{F}_{E_E}(xy)$ respectively. This is not surprising as we know that y-axis forces have different patterns in different interaction behaviors, especially in CT where the main exerted forces by the partners are in x and z-direction (i.e., $F_{S_Y} = F_{E_Y} \approx 0$). As a result, adding such features increase the classification accuracy to distinguish CT from other behaviors (see Figure 2.13(c)).

Negotiation torque efficiency about x-axis, $M^{\tau}_{NE}(x)$, occupy the 11th important rank. This feature represents the ratio of the net torque applied on the object about x-axis divided by the norm of the effective applied torque by the partners about that axis (i.e., the x-axis). Therefore, following the same explanation for $M^{\tau}_{TE}(x)$ above, this feature (i.e., $M^{\tau}_{NE}(x)$) can be informative in differentiating HR from other behaviors.

Since the forces in z-direction also have a unique pattern in CT, it was not surprising that the force-related metrics in *x*-*z* plane $M^{F}_{E_E}(xz)$, $M^{F}_{E_S}(xz)$, and $M^{F}_{TE}(xz)$ have important weights and come in 7th, 8th, and 12th importance ranks, respectively.

Our haptic metrics can be categorized in to two groups; those that include information about the forces/torques in the considered plane only (i.e., negotiation efficiency and similarity); and those that carry the force/torque information in the considered plane with respect to total forces/torques applied by the partners in 3D (i.e., individual efficiency and team efficiency). Looking at Table 2.4, we can clearly say that the metrics in the latter category are in general more significant than those in the first category. For instance, it is shown that force negotiation efficiency in x-y plane (28^{th}), and in x-z plane (29^{th}) and the similarity in torques about y-axis have zero weight, as these features hold no distinct information throughout all interaction patterns.

Chapter 3:

RESOLVING CONFLICTS DURING HUMAN-ROBOT CO-MANIPULATION

In this chapter, we aim at adjusting a robot's behavior to adaptively cooperate with a human while performing an object manipulation task. To achieve this, we propose an approach that enables the robot to detect the dyadic interaction behaviors emerge during the execution of the co-manipulation task. Compared to the earlier studies, we focus on dyadic behaviors rather than human intention alone. We utilize features derived from haptic data only as inputs to a machine learning algorithm to detect if both robot and human translate the object harmoniously or they face a conflict. Accordingly, a robot can act as a follower to a human partner or lead the task proactively in response to the detected interaction behaviors. For this purpose, we implement an admittance controller to make the robot behave proactively, and an artificial potential field approach to define the trajectory for the proactive robot. We designed experimental scenarios to build the learning model, and then we utilized this model in a pHRI co-manipulating task to verify our proposed algorithm.

3.1 *Approach*

In this part, we focus on conflict-driven dyadic interaction patterns that typically emerge during co-manipulation. In our pHRI scenario, the human and the robot collaborate to jointly move an object (see Figure 3.1) toward a target location. Our approach detects interaction patterns using a random forest classifier, which is a supervised ML classification algorithm, and adapts the robot's role accordingly.

Figure 3.2. presents a flowchart to summarize our approach: Initially, the robot passively follows the movements of the human based on the magnitude and direction of the forces applied by him/her, since it is not given the target location. Once the direction of human force vector settles (see Section 3.1.3), robot estimates an intended target location by intersecting a line in the direction of human force vector with a virtual boundary defined by a virtual circular workspace defined around the robot. An artificial potential field (APF) is generated to compute a trajectory for the robot to move the object towards the estimated target location. At this stage, the robot becomes proactive and moves the manipulated object collaboratively with the human partner. If the human changes the target during this manipulation, a conflict arises.

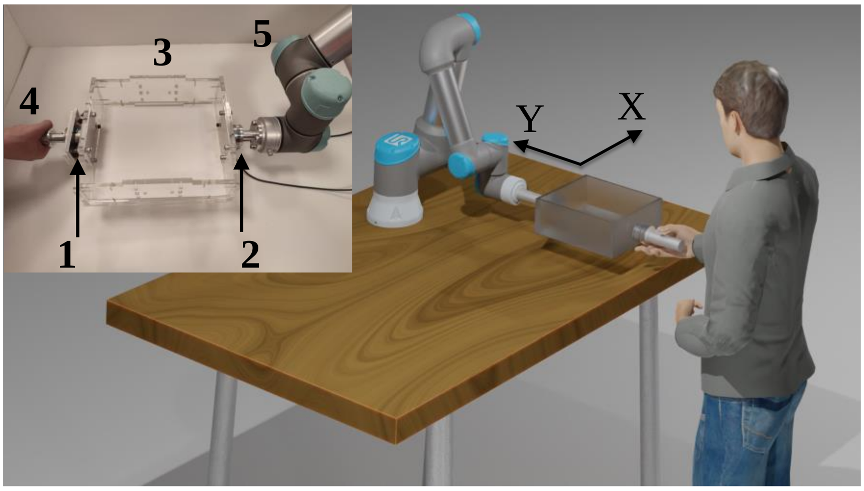

Figure 3.1: Human-robot co-manipulation scenario. Upper left figure shows the force sensors attached to the object for measuring the forces applied by human (1) and robot (2), the actual object being manipulated (3), human hand (4), and our collaborative robot (5).

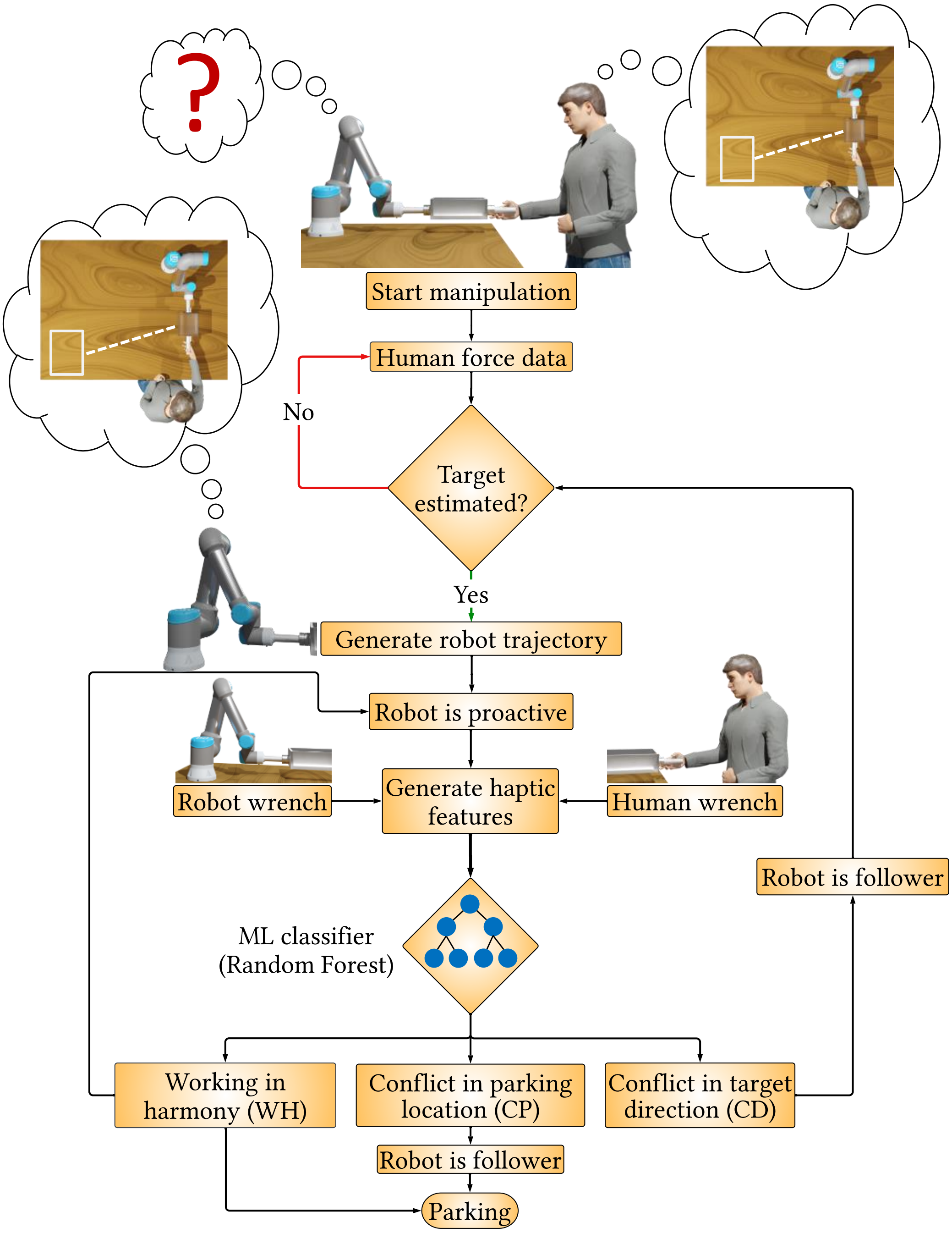

Figure 3.2: The flowchart of the proposed pHRI approach for co-manipulation of an object.

We use a random forest ML model, trained with haptic-related features derived from the forces/torques (i.e., wrenches) applied on the object, to detect three interaction patterns:

1) WH: Working in Harmony: The partners agree on the target direction; hence, they move the object harmoniously.

2) CD: Conflict in target Direction: The partners face a conflict in movement direction as each aims at a different target location.

3) CP: Conflict in Parking location: The partners face a conflict in parking location since one of them aims to stop the motion of the object before or after the intended/estimated target location.

The random forest ML classifier detects these behaviors and notifies the interaction controller of the robot to generate a suitable response as shown in Figure 3.2. If WH pattern is detected, the controller maintains the proactive status of robot.

On the other hand, if CD is detected, the controller switches the robot role to a follower until a new target location is determined and a new trajectory is generated. In CP, robot relinquishes its trajectory and acts as a follower to assist the human in parking the object. To avoid any jerky motion in CD and CP due to the switching between robot states, we gradually scale down the robot's attractive force in APF to zero once the robot turns from a proactive state to a passive state.

3.1.1 Hardware Setup

The setup used in our experiments (see Figure 3.1) consists of a UR5 collaborative robot, a box-shaped object made of plexiglass with dimensions of 30 cm × 25 cm × 10 cm and a weight of 2.5 kg, two force/torque (F/T) sensors (Mini45, ATI Inc.), and a computer screen to provide visual feedback for the participants. This setup physically couples the human and the robot through the manipulated object. One end of the object is rigidly connected to the robot via an F/T sensor to measure the wrenches applied by the robot. Human holds the object from the opposing end through an aluminum handle. A F/T sensor is attached to this handle to measure the human wrenches. All data is acquired at 125 Hz by an external DAQ card (USB-6343, National Instruments Inc.), connected to a personal computer.

3.1.2 Control Architecture

The control architecture utilized in this study is shown in Figure 3.3. An admittance controller regulates the interactions between the human and the robot. Initially, the target location is unknown to robot, which starts as a follower.

At this stage, the ML classifier is not active, and only the human force, F_H, is fed to the admittance controller to generate the reference velocity V_{REF} for the robot's motion controller, which in turn, transmits torques to robot joints to move the object with velocity V. Once the target location is estimated by the robot based on the direction of human force, a trajectory is generated for the robot using the APF and the robot is pulled to the estimated target location with an attractive force F_{ATT} (we assume no obstacles in the environment, hence the repulsive force is always set to zero in this study). Here, the force applied by human partner F_H is added to F_{ATT} and the total force F_T is sent to the admittance controller. At this stage, ML classifier is active and utilizes the haptic-related features computed using the wrenches applied by human and robot (W_H and W_R) on the object, to predict the interaction pattern. If WH is detected, the robot contributes to the task proactively. On the other hand, if CD or CP is detected, the robot switches its role to a follower.

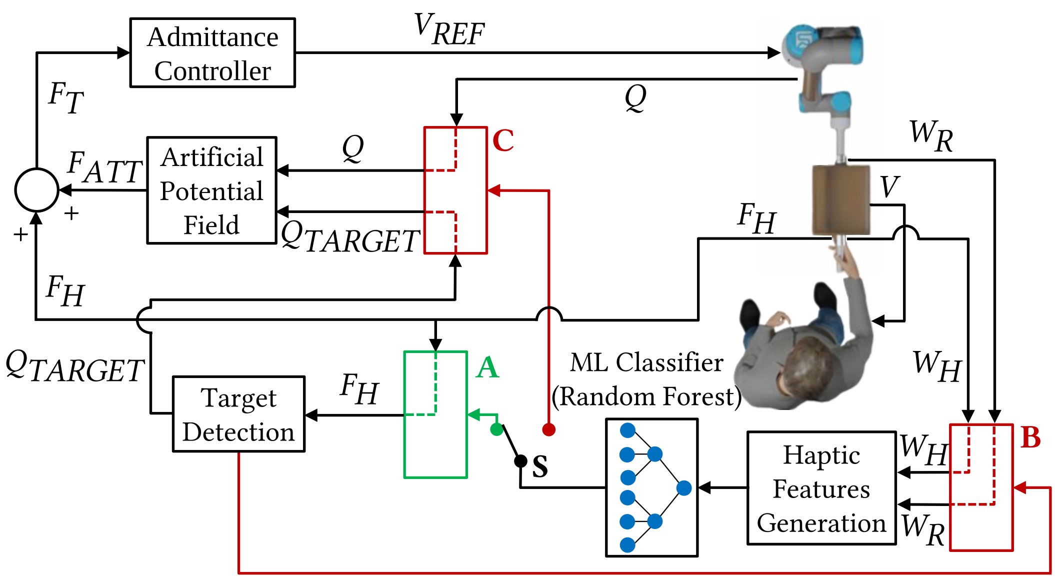

Figure 3.3: The control architecture utilized in our pHRI approach to regulate the harmonious and conflicting interactions between human and robot.

Role switching: Figure 3.3 includes logical commands to activate central input lines to turn on the data flow for blocks A, B, and C. The two-way switch S turns on block A while deactivating block C (i.e., robot is a follower), which is the starting phase of the motion in our approach. Similarly, if target location is determined, block B is activated; hence machine learning is involved. Consequently, switch S, which works based on the classifier decision, activates block C whenever WH pattern is detected. On the other hand, if the ML classifier observes one of the conflicting patterns (CD or CP), block C is deactivated by switch S, and the robot is a follower again.

Admittance Controller: The transfer function model of the admittance controller utilized in this study is similar to that in [31]:

$$Y(s) = \frac{V_{REF}(s)}{F_T(s)} = \frac{K_A}{\tau_A s + 1} \tag{3.1}$$

where, K_A and τ_A are the admittance gain and time constant, respectively, $V_{REF}(s)$ and $F_T(s)$ are respectively the Laplace transformations of the reference velocity and the total force.

3.1.3 Trajectory Generation

We utilize an APF (artificial potential field) to generate a trajectory for the robot, to be used when it proactively cooperates with the human partner. In APF, the total potential field $U(Q)$ is made of an attractive, $U_{ATT}(Q)$, and a repulsive, $U_{REP}(Q)$, field [51]. In our scenario, there are no physical obstacles in the environment, hence we ignore the repulsive field. However, even if there were obstacles, the proposed paradigm would have worked without needing any modifications: The human could perceive the environment and direct the motion to avoid obstacles, while the robot reacts to detected conflicts.

The total force, which defines the robot’s contribution to the task, is calculated as the negative gradient of the total potential field, $F_{ATT} = -\nabla U(Q) = -\nabla U_{ATT}$. This attractive force is set at its maximum value when the robot is fully proactive, and gradually reduces to zero as it reaches the target.

To implement the APF, the position of the target Q_{TARGET} should be known by the robot. However, estimating the intended target location at the very beginning of the movement, which is only known by human, is not trivial.

In our approach, initially, robot has no prior information about the target location; hence it starts the task as a follower while human guides it toward the target by applying forces to the manipulated object. Once the direction of the human force vector settles toward a specific direction, robot utilizes this direction to estimate the target location by intersecting the vector of human force with a virtual circular task boundary within the robot workspace, centered around the robot base frame. To decide that the human's forces settle on a direction, we first measure the angle *(θ)* between the human force vector and the x-axis of robot. Then, we select a sliding buffer of size *n* for the measured data and compute the mean of the absolute differences between the angles in this buffer and their average. When this mean value is less than a threshold value (i.e., $(\sum_{i=1}^{n}|\theta_i - \theta_{AVE}|/n) < \theta_{THR}$), we consider that the human force vector settled in the desired direction without considerable deviation. Note that when human changes the target location by altering the movement direction during the manipulation while robot is still active and moves toward the initial target, conflict in target direction (i.e., CD) emerges. Once robot detects this conflict, it leaves its own trajectory and follows the human passively until it can estimate the new target location and generate a new trajectory.

To avoid high attractive forces far from the target, we utilize a hybrid APF that uses quadratic potentials near the target and a conic formula when farther away as illustrated in Figure 3.4 [51]:

$$F_{ATT} = \begin{cases} -\xi(Q - Q_{TARGET}) & \text{if } \rho_{TARGET}(Q) \le d_t \\ -d_t\,\xi\,\dfrac{(Q - Q_{TARGET})}{\rho_{TARGET}(Q)} & \text{if } l - d_s > \rho_{TARGET}(Q) > d_t \\ -d_t\,\xi\,\dfrac{(Q - Q_{TARGET})}{\rho_{TARGET}(Q)}\,m & \text{if } \rho_{TARGET}(Q) \ge l - d_s \end{cases} \tag{3.2}$$

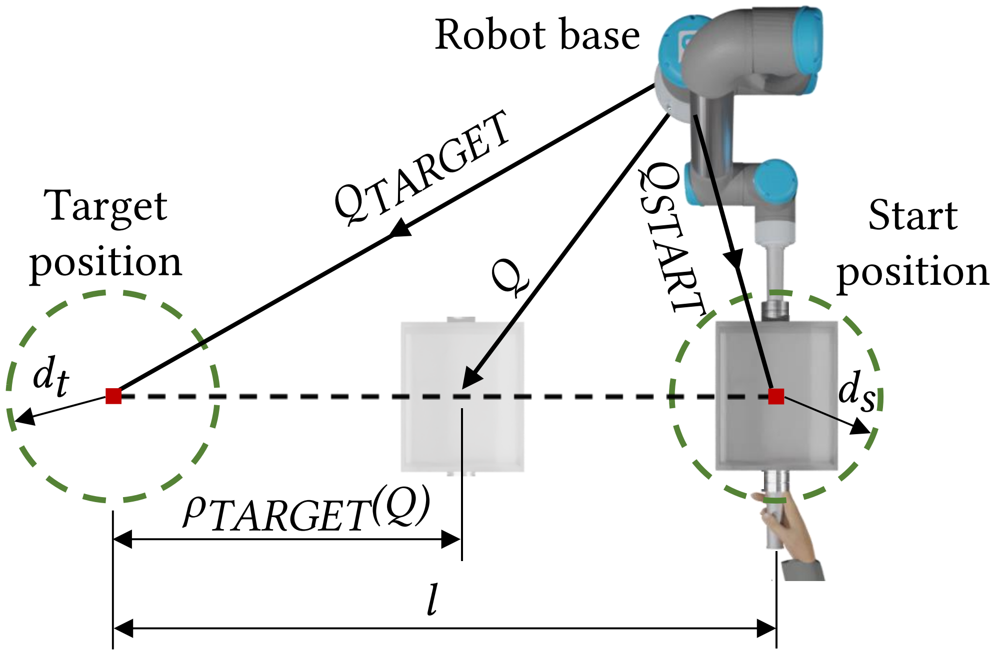

Figure 3.4: The parameters used for implementing the attractive potential field.

where ξ is a positive constant scaling factor, Q and Q_{TARGET} are respectively the current and target position vectors of the object with respect to the robot base frame, d_t is a positive constant to define a catchment area around the target for switching between quadratic and conic formulas, and $\rho_{TARGET}(Q)$ is the Euclidean distance to target $\|Q - Q_{TARGET}\|$.

To prevent the attractive force from being set to its maximum value, $F_{ATT} = d_t\, \xi$, at the beginning of the task, which would cause a jerky motion, we introduced three new variables as shown in Figure 3.4: $l = \|Q_{START} - Q_{TARGET}\|$ is the Euclidian distance between the object's starting position vector, Q_{START} and the estimated target, d_s is a distance threshold around Q_{START}, and $m = \left(\left(d_s - \rho_{START}(Q)\right)/l\right) + \left(\rho_{START}(Q)\right)/d_s$ is a scaling constant, where $\rho_{START}(Q) = \|Q - Q_{START}\|$.

3.2 *Experiments*

In order to train and validate our ML classifier, we designed and implemented two sets of pHRI experiments:

1) Training Experiments: These experiments were designed to train and test the ML time-series classifier, relying on haptic features for distinguishing between the human-robot interaction behaviors.

2) Validation Experiments: These experiments were designed to investigate the potential benefits of the proposed ML approach in comparison to two other approaches.

All experiments utilized the same setup shown in Figure 3.1. The object manipulations mainly involved translation and performed in the xy plane. The experimental study was approved by the Ethical Committee for Human Participants of Koc University. The values of the parameters used in the implementation were selected as; $K_A = 0.0167$, $\tau_A = 0.054$, $n = 30$, $d_t = 8$ cm, $d_s = 4$ cm, $\xi = 125$, and $\theta_{THR} = 0.08$ rad.

3.2.1 Training Experiments

3.2.1.1 Training Scenarios

The objective in designing the training scenarios was to collect haptic data to train a classifier model that can effectively distinguish between different interaction patterns (WH, CD, CP).

To this end, 16 different manipulation scenarios, listed in Table 3.1, were introduced by covering as many different combinations of interaction behaviors as possible without being too exhaustive. In these training scenarios (TS), human and robot collaborate to move the object from the starting location to one of the target locations shown in Figure 3.5 (A, B, C, D, E, F). In designing these scenarios, we intentionally created harmonious and conflicting patterns by assigning a specific target location for the robot and hence a trajectory to follow, regardless of the human partner's target location. As a result, harmonious/conflicting interaction patterns resulted from the agreement/disagreement between the partners.

To put things into context, consider training scenario 8 in Table 3.1, where both the human and the robot have the same target direction but different locations; therefore, they are expected to work in harmony (WH) initially to move the object toward that direction. However, as the human's scenario requires him/her to park the object (at target F in Figure 3.5) before the robot's target (target E in Figure 3.5), they face a conflict in parking location, CP.

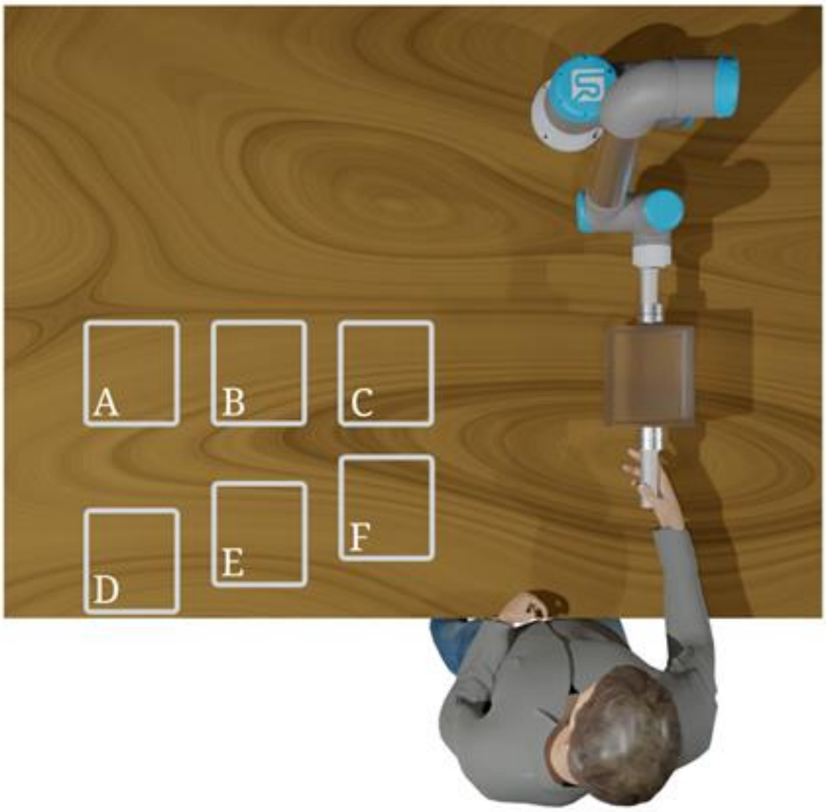

Figure 3.5: Scenarios used in training experiments.

3.2.1.2 Participants and Protocol

The training experiments were performed with 8 subjects (2 females and 6 males with an average age of 26.25 ± 4.2 SD). Prior to the experiment, subjects were instructed about the experimental procedure. They were not aware of the robot's target and explicitly instructed to move the object toward their own targets regardless of robot's behavior. Subjects performed the task by following the text instructions and visual images displayed on a computer screen, and the software sounds played during the experiment. To familiarize themselves with the setup, all subjects performed one manipulation trial involving harmonious collaboration (WH) with the robot. Thereafter, each subject performed the scenarios listed in Table 3.1 in four separate sessions with 5 minutes break between the sessions. Each subject performed 32 trials, where each scenario repeated twice. The order of the scenarios was randomized in each session, while the order for all subjects was the same.

Table 3.1: Training scenarios and the expected interaction behaviors

Training scenario (TS)	Robot target	Human target		Expected behavior
		Initial	Final	
TS1	B	B	B	WH
TS2	E	E	E	WH
TS3	B	E	E	CD
TS4	E	B	B	CD
TS5	B	A	A	WH, CP
TS6	B	C	C	WH, CP
TS7	E	D	D	WH, CP
TS8	E	F	F	WH, CP
TS9	B	B	F	WH, CD
TS10	E	E	B	WH, CD
TS11	E	B	D	CD, WH, CP
TS12	E	B	F	CD, WH, CP
TS13	B	E	A	CD, WH, CP
TS14	B	E	C	CD, WH, CP
TS15	E	B	E	CD, WH
TS16	B	E	B	CD, WH

Subjects started the experiment by grasping the object from their handle while facing the robot handling the object from the other side by its end effector. To provide visual feedback to the subjects, initial and target locations were displayed on the computer screen as static 2D rectangles in white color while the current location of the manipulated object was displayed as a moving 2D rectangle in pink. A message was displayed on the screen along with a distinct software sound to notify subjects to start the task. During the task, if the scenario involved a change in target location, the new target location was updated immediately on the screen to notify the subject. When the subject reached the target, the color of the rectangle at the target changed to green to notify the subject, and after staying at the target for 2 seconds, a message appeared on the screen along with a distinct beep to inform the subject about successfully parking the object.

3.2.1.3 Haptic Features and Classifier Design

The raw haptic data (i.e., wrenches applied by human and robot) collected during the training experiments are annotated and segmented based on the expected behaviors listed in Table 3.1 by following the procedure employed in Chapter 2. As demonstrated in this work, the features extracted from the haptic data alone are sufficient to distinguish between different interaction patterns. We utilize the haptic features, originally suggested by Noohi and Žefran [16] and extended in Chapter 2, see our earlier publication Al-Saadi et al. [52], to train our random forest ML classifier. We briefly mention them here for the sake of discussion, but the details are available in Section 2.3.

Consider Figure 3.6, where F_H, F_R , and F_{SUM} are the forces applied on an object by the human and the robot, and the summation of these forces, respectively. That is:

$$F_{SUM}(t) = F_H(t) + F_R(t) \tag{3.3}$$

The effective forces of human F_H^* and robot F_R^* that contribute to the task are calculated as the projection of partners' forces on F_{SUM}:

$$F_H^*(t) = \alpha \, F_{SUM}(t) \tag{3.4}$$

$$F_R^*(t) = \beta \, F_{SUM}(t) \tag{3.5}$$

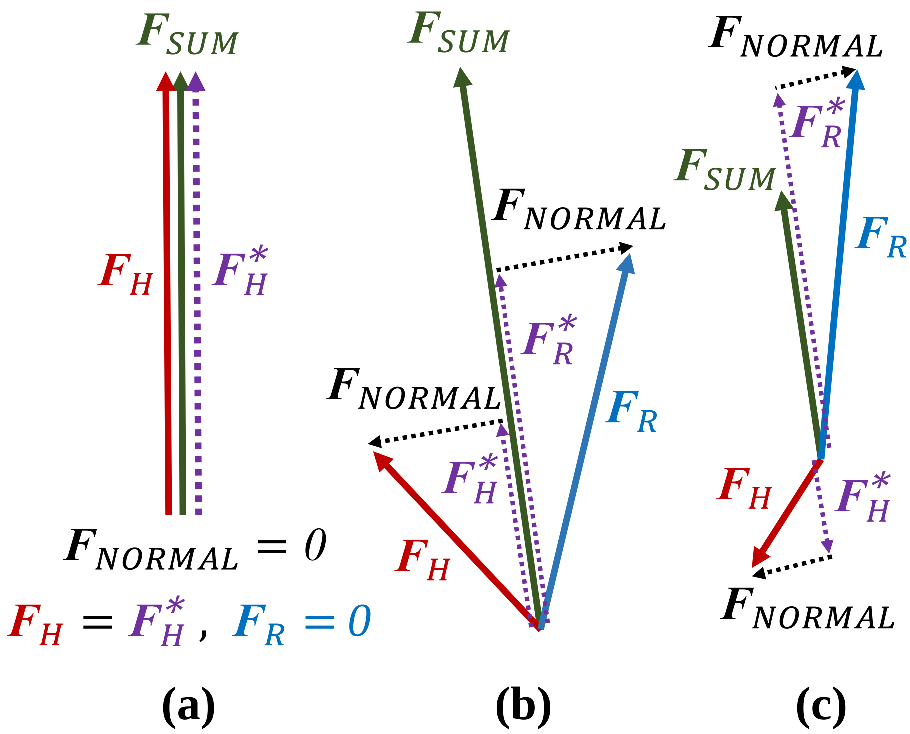

Figure 3.6: Force decomposition. F_H, F_R, F_{SUM} are human applied force, robot applied force, and their summation, respectively. F_H^*, F_R^* are the human and robot effective forces, respectively. F_{NORMAL} are the normal force that is perpendicular to F_{SUM}.

where t is the time step and $\alpha + \beta = 1$. The forces that are perpendicular to F_{SUM} (i.e., F_{NORMAL} in Figure 3.6) do not contribute to the task and are canceled out.

Based on this force decomposition, five force-related features were introduced: individual force efficiencies $M_{E_K}^F$, team force efficiency M_{TE}^F, negotiation force efficiency M_{NE}^F, and similarity of forces M_S^F. In addition, five additional torque-related features were introduced [52]: individual torque efficiencies $M_{E_K}^\tau$, team torque efficiency M_{TE}^τ, negotiation torque efficiency M_{NE}^τ, and similarity of torques M_S^τ. Note that the subscript K in $M_{E_K}^F$ and $M_{E_K}^\tau$ refers to either human (*H)* or robot (*R*), while the superscripts F and τ refer to force and torque-related features, respectively.

In Chapter 2, we showed that analyzing the task in different movement planes resulted in more informative features than analyzing it in 6-DoF space. For that, we performed the force/torque decomposition in the three principal movement planes, *xy*, *xz*, and *yz*. This resulted with 30 wrench-related features (10 wrench-related features × 3 planes) that are used as inputs into our classifier. We utilized a random forest algorithm to train our time-series classifier model to discriminate between the interaction patterns. Random forest is a supervised learning algorithm used for both regression and classification. In classification, it constructs a multitude of decision trees and outputs the class selected by most of them. Python Scikit-Learn package was utilized for the implementation of the algorithm [50]. The number of trees in the random forest was set to 100 while the maximum depth of the trees was unconstrained.

We split the dataset into two distinct sets: training and test. To train the classification model, we used the data coming from 24 trials of each subject and used the remaining 8 trials for testing. Since there were 8 subjects, the total number of trials for training and testing were 192 (75%) and 64 (25%), respectively. We achieved a classification accuracy of 88.82% and a BER of 0.11 after cross-validation. Figure 3.7 shows the confusion matrix.

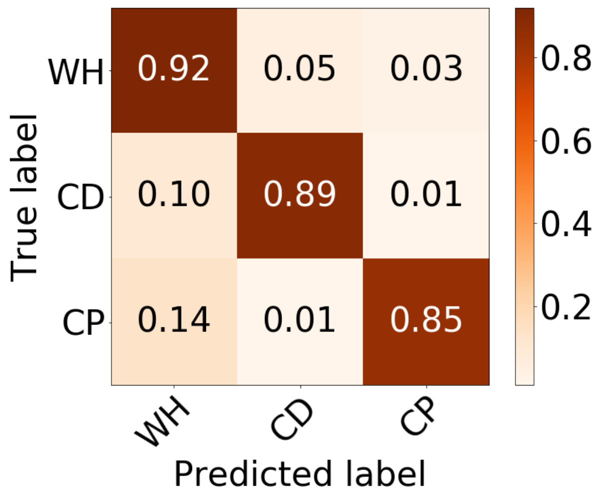

Figure 3.7: Confusion matrix for classifier trained with haptic feature set. WH, CD, and CP are working in harmony, conflict in target direction location, and conflict in parking location.

3.2.2 Validation Experiments

To evaluate the performance of our proposed approach, we implemented another set of experiments utilizing the same setup and scenarios. Recalling the co-manipulation example discussed in the introduction section, where the robot acts either as a follower or interacts proactively with human, we considered 3 experimental conditions (C1, C2, and C3). The first condition, C1, implements a simple leader-follower model where the robot is passive and always follows the human. In C2, the robot has a fixed target location and follows a trajectory based on the APF, regardless of the agreement/disagreement with human partner. In C2, the robot assists the human partner (i.e., contributes to the task) if they have the same target. Nevertheless, when they are given different target locations, they display conflicting behaviors, which cannot be resolved. Finally, C3 utilizes our approach of integrating the APF with the ML classifier for conflict resolution.

Three different experimental scenarios (ES1, ES2, and ES3) were considered for the validation experiments (Figure 3.8). In ES1, human and robot work in harmony (WH) to transport the object to a target position (point B), while in ES2, the target location changes suddenly from location B to location E, causing a conflict in movement direction (CD). Finally, in ES3, the target location suddenly changes from location B to location C, causing a conflict in parking location (CP).

Six subjects, with an average age of 25.5 ± 4.4 SD, participated in this experiment. Each experimental condition (C1, C2, and C3) was repeated twice for each experimental scenario (ES1, ES2, and ES3). Hence, the total number of trials performed by each subject was 18, which were completed in two sessions with 5 minutes break between the sessions. The order of the experimental conditions and scenarios was randomized in each session while the same order was displayed to each participant.

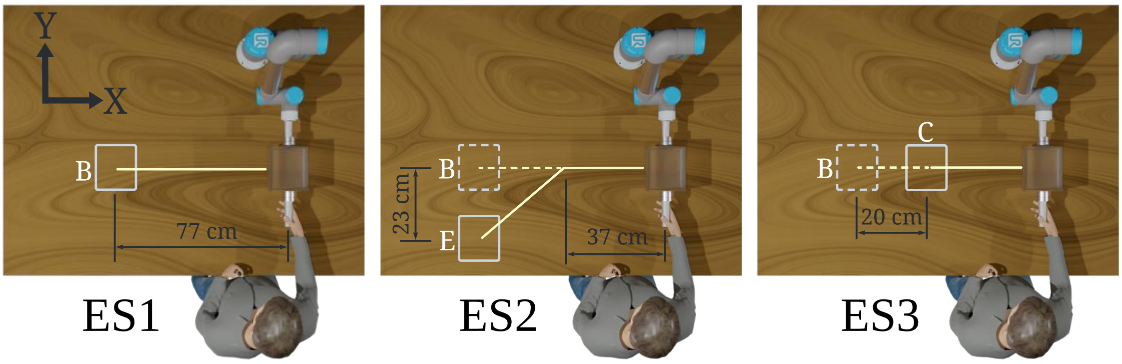

Figure 3.8: Experimental scenarios (ES) used in validation experiments.

3.2.2.1 Results and Discussions

3.2.2.1.1 Force Profiles and Classifier Performance

Figure 3.9 represents the force profiles of a representative dyad (a human and a robot) for ES1, ES2, and ES3 under C3 (our approach) in tandem with the decisions taken by the classifier. We concentrated on the forces applied in the *xy* plane, which is the plane of most movements in our experiment.

In all plots, subscripts H and R stand for human and robot, respectively. The blue and red lines in Figure 3.9a represent the forces applied by human and robot, respectively (please note that all forces were presented with respect to the manipulated object frame), while Figure 3.9b depicts the raw predictions RP (green vertical lines) and processed predictions PP (orange line) of the ML classifier. As shown in Figure 3.9b, the classifier successfully predicted the interaction behaviors in all experimental scenarios. Moreover, the classifier was able to predict the conflicting behaviors (i.e., CD in ES2 and CP in ES3), which occurred for short periods of time only, and instructed the controller to resolve the conflicts by switching the robot to a follower state. Prior to sending the classifier decision to the controller, a voting buffer was implemented:

Voting buffer. This buffer uses raw predictions within a window of 20 samples, with an overlap of 10 samples between each buffer, and outputs the most frequent prediction in the buffer. The behavior predictions are processed every 10 samples. Using this buffer eliminates instantaneous misclassifications due to the sudden and unintentional movements. For instance, in Figure 9b, some patterns were misclassified initially (i.e., a CP in ES2 and some CDs in ES1), but these were filtered out by the voting buffer. By inspecting the interaction behaviors in Figure 3.9, we observed that they produced highly complex force profiles though the object manipulations were translational (no rotations) and mainly performed in the xy plane. For example, the yellow-colored shaded areas in Figure 3.9 correspond to WH behavior, in which the partners harmoniously translated the object toward the target. One anticipates that partners perform the manipulation by exerting forces in the same direction of the movement during this type of interaction. However, when the force profiles in Figure 3.9a are inspected carefully, one observes that only human partner applies forces in the direction of the movement while the forces applied by robot are in the opposite direction. The reason for this mismatch is due to the delay in the reaction times of the partners to each other's actions as also observed in human dyads [52].

The grey-colored shaded area in Figure 3.9 corresponds to CD behavior, in which the partners disagreed on the target direction. This behavior occurred in ES2 scenario: a new target location (location E in Figure 3.8) was suddenly displayed to the subject, and he/she started to apply forces in the negative y-axis to move the object toward the new target. As the robot was still actively moving toward the original target location (location B in Figure 3.8), it resisted human movement, which resulted in the opposing forces applied by the partners along the y-axis. By inspecting the force patterns during this behavior, we observed that they changed in both x and y directions, although the new target position deviated from the initial one along the y-direction only.

Finally, in CP behavior (the pink-colored shaded area in Figure 3.9), the subject and the robot were given the same target location of B as shown in ES3 in Figure 9, but the subject was instructed later to park the object suddenly at location C prior to reaching the original target location at B. Subject applied forces in opposite direction to the movement (along x-axis) to park the object at location C, as clearly shown in Figure 3.9a for ES3 (see the change in the direction of forces in the pink shaded region). However, since the robot was moving the object toward B, it applied forces opposite to the direction of forces applied by the subject.

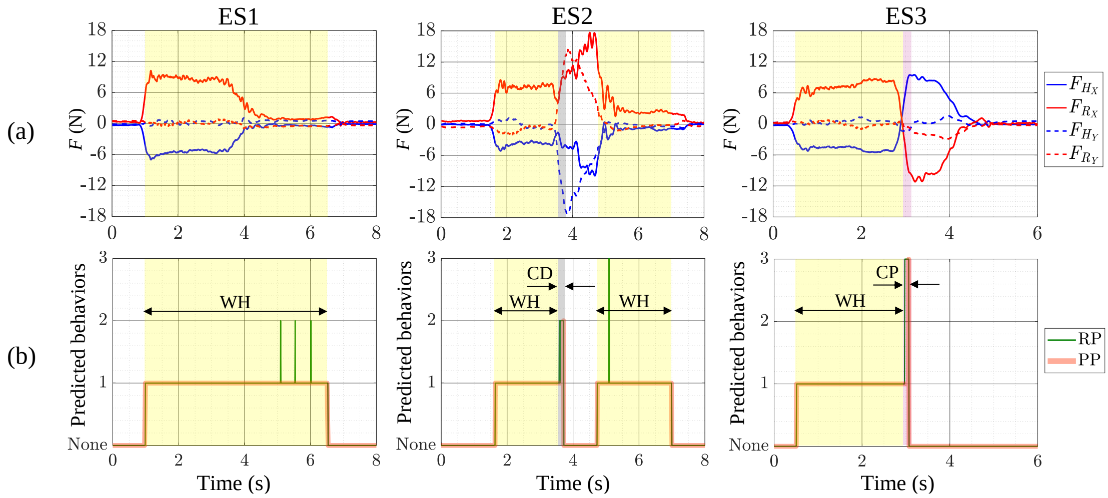

Figure 3.9: (a) Forces profiles of a human subject (blue) and robot (red), and (b) the raw predictions (RP) by ML and the processed predictions (PP) after filtering for the experimental scenarios ES1, ES2, and ES3 under our proposed approach (C3). Subscripts H and R stand for human, robot, respectively. The predicted values 1, 2, and 3 stand for WH, CD, and CP interaction behaviors, respectively, while "None" stands for the periods where ML is inactive, and the robot is follower.

The observations above reveal the complexity of the force signals though the task was implemented in 2D. This infers that generating rules based on force signals to distinguish between these behaviors is not straightforward, especially when the task is conducted in 6D. Hence, the ML approach proposed in this paper has more generalization potential to identify similar behaviors.

3.2.2.1.1 Task Performance Under C1, C2, and C3

We used the following metrics [31, 53] to evaluate the task performance of the subjects: the average velocity of the object ($V^{\text{AVE}} = 1/(t_f - t_i) \int_{t_i}^{t_f} |V(t)|\, dt$), average force applied by subject ($F_H^{\text{AVE}} = 1/(t_f - t_i) \int_{t_i}^{t_f} |F_H(t)|\, dt$), average power consumed by the human ($P^{\text{AVE}} = 1/(t_f - t_i) \int_{t_i}^{t_f} |F_H(t).V(t)|\, dt$), and the task completion time (TCT). Here, t_i and t_f are the timestamps when the object velocity just exceeded 2% of the maximal velocity (denoting the start of the trial) and the ending time of the trial, respectively. TCT was computed as $t_f - t_i$.

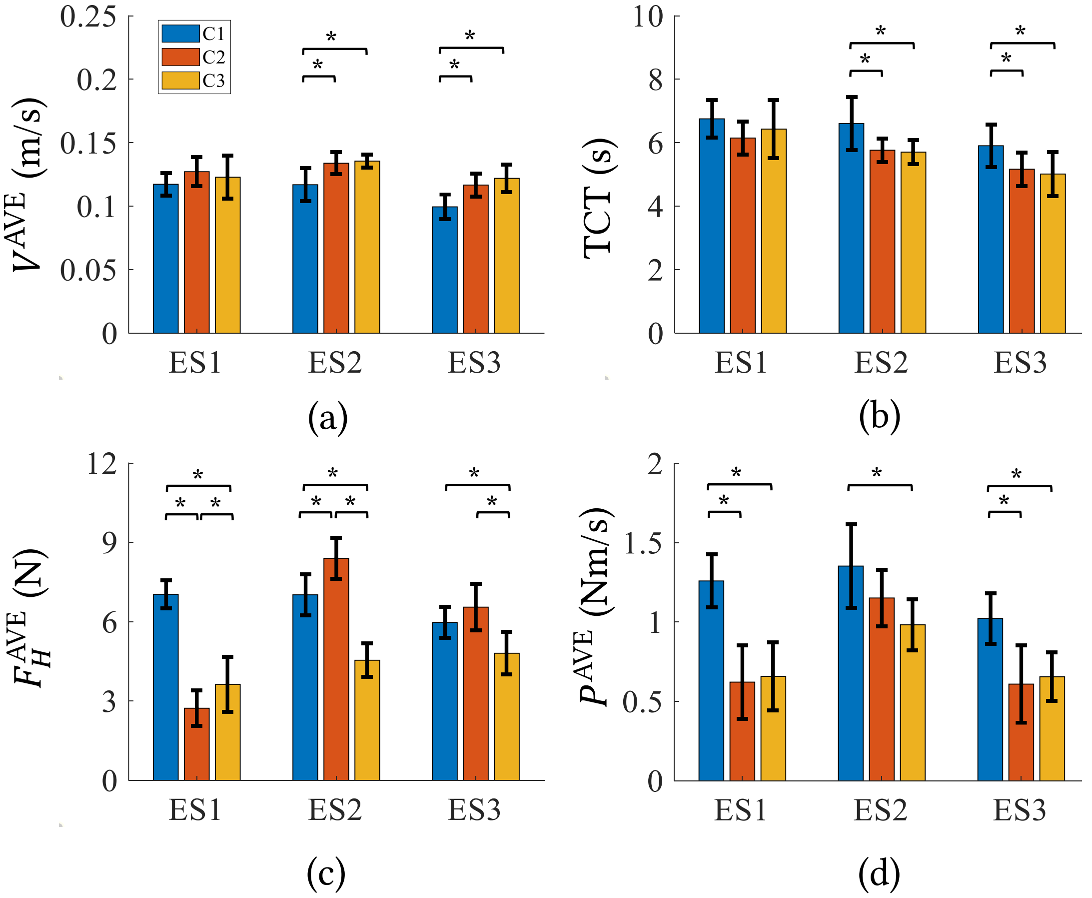

Figure 3.10: Mean values of the performance metrics for three experimental scenarios ES1, ES2, and ES3 under three different experimental conditions C1, C2, and C3. Error bars are the standard deviations of means and horizontal bracket with * on top indicates statistically significance pairwise comparisons with p = 0.05.

Figure 3.10 presents the means and standard errors of means of the performance metrics of the subjects under each experimental condition (C1, C2, and C3) for each scenario. We performed a one-way ANOVA with Tukey corrected post-hoc tests to examine the effects of the experimental conditions on the performance metrics.

Figure 3.10a (3.10b) shows that V^{AVE} (TCT) under C2 and C3 were significantly higher (lower) than that of C1 in both ES2 and ES3. Although V^{AVE} (TCT) under C2 and

C3 were higher (lower) than that of C1 in ES1, the difference was not statistically significant. In addition, the differences in V^{AVE} and TCT between C2 and C3 were not significant in any experimental scenario.

In Figure 3.10c, we observe that the average forces applied by subjects F_H^{AVE} under C3 (our proposed approach) were significantly lower than those of C1 and C2 in both ES2 and ES3, and lower than that of C1 in ES1. In addition, F_H^{AVE} under C2 was lower than those of C1 and C3 in ES1. This shows that the ML classifier in our proposed approach (C3) successfully resolved the conflicts between human and robot, and hence reduced the forces exerted by human to change the direction of movement or parking location. Additionally, F_H^{AVE} under C2 was higher than those of C1 in both ES2 and ES3. Although the APF utilized in C2 reduced the task completion time compared to C1, it caused the subjects to exert more force during the conflicting scenarios in ES2 and ES3.

Figure 3.10d shows that subjects spent less effort P^{AVE} under C2 and C3 compared to that under C1 due to the benefit of utilizing APF, especially in ES1. Moreover, when the conflict was stronger, as in ES2, C3 led to less effort than that of C2, thanks to our ML model in resolving the conflict. The results on P^{AVE} showed that the conflicts in parking (ES3) were more easily (with less effort) resolved than the conflicts in changing direction (ES2).

In summary, our proposed approach C3 resolved the conflicts between the partners effectively, allowing subjects to exert less force than those under C1 and C2. However, in ES1, where no conflict happened, we can see that F_H^{AVE} under C3 was higher than that of C2. This is because the robot in C2 was active through the whole task, while in C3, human needs to apply forces to guide the robot as it starts the task as a follower. Although subjects applied less force under C3, they translated the object with higher velocities and lower TCT (particularly compared to those under C1). The results of the experiments show that our approach (C3) reduces the average force applied by subjects by 42.65% and 30.6% compared to those under C1 and C2, respectively. Moreover, the average power spent by the subjects under C3 was reduced by 46.27% and 4.94% compared to those of C1 and C2, respectively.

Chapter 4:

CONCLUSION

In the first part of this dissertation, we tested our hypothesis that haptics-related features would be sufficient to distinguish between interactive behavior patterns. This behavior information will be useful when programming a robot partner that reads interaction states and reactively acts in response to the predicted behaviors, which is the ultimate goal of this research.

We designed and conducted a pHHI experiment with 12 subjects and investigated conflict-driven interaction behaviors under six task scenarios. We proposed a wrench-based feature set, inspired by the work of Noohi and Žefran [16], to classify the interaction behaviors. Using a random forest classifier, we verified that haptic information, i.e., wrenches, was sufficient to differentiate between the interaction patterns. This contrasts with earlier work [25], [26], which suggested that kinematic information is needed to improve classification rates in distinguishing between interaction patterns in dyadic co-manipulation. In this work, we have demonstrated that using carefully devised haptic-related metrics derived from raw data eliminates the dependency on kinematics. This result is very important in designing future studies as it removes the necessity for tracking object motion when trying to understand the interaction states.

Another contribution of this work is our task analysis in different movement planes. By decomposing the motion in the object frame, we could eliminate the dominant forces for lifting motion, which would otherwise be interfering with the classification results. The proposed force decomposition method allowed more informative features to be extracted from raw data.

This study focuses on designing interaction-specific haptic features to identify conflict-related behaviors during a continuous physical human-human collaborative task. Our results provide important insight into the amount of information that is carried over haptics in physical co-manipulation. Although this work only presents an evaluation of pHHI behaviors, its outcomes were utilized to design proactive collaborative robots, which are aware of the interaction states during the tasks, as we introduced in the second part of this dissertation.

In this experiment, we constrained the subjects to a single scenario and asked them to concede to the experimenter's motion if they feel a conflict. This was done to avoid implicit role allocations between partners, and ease the data annotation process in our experiment. However, role definitions are key in human interactions and were demonstrated to be effective mechanisms to improve collaboration in earlier work [7], [33], [34]. In future work, we plan to explore online interaction behavior classification as a way to investigate how conflicts arise and are resolved if subjects are also allowed to take on leadership roles.

In the second part of this dissertation, we proposed an approach that allows the robot to proactively interact with a human partner based on the time-series classification of the interaction behaviors that arise while executing a continuous pHRI collaborative task. During these interactions, conflicts may naturally arise if the partners have different movement intentions. To resolve these conflicts, we argue that it is important to study the dyadic interaction behaviors rather than the individual behavior of human partner. Moreover, we show that the features derived from haptic data alone are sufficient to detect these conflicts. These features were used to train a random forest classifier that differentiates between the interaction patterns.

To demonstrate our approach, we designed a pHRI experiment where both human and robot collaborated to manipulate an object. Experimental scenarios that involve partners work in harmony and conflict with each other in movement direction and parking location were designed to test the efficacy of the proposed approach. The results showed that our ML classifier successfully recognized the interaction behaviors that emerged during those scenarios and instructed the robot to take proper action accordingly. Hence, the robot was able to adapt its behavior to act as a follower when there was a conflict or contribute to the task proactively when the dyad was working in harmony. As a result, the conflicts between human and robot during the manipulation were accommodated effectively and the subjects performed the task with lower effort.

Our current experimental scenarios involved translational manipulations of an object in 2D space. As a future work, we aim to extend our approach to more complex scenarios involving object manipulations in 6D space. In particular, we would like to show that a rule-based approach (e.g., defining some rules based on force magnitudes/thresholds) cannot successfully detect conflicts in such complex manipulation scenarios, or the same rules cannot be applied easily to other manipulation scenarios involving different sub-tasks or objects having different shape, weights or material properties (e.g., elastic objects). Additionally, we would like to design a questionnaire, similar to that done in [54], to measure the perceptions of human subjects participating in our experiments about their sense of interaction with the robot under different experimental conditions and scenarios. We are interested in quantifying the degree of conflict that they subjectively feel in the presence of a proactive robot and how much of our approaches help humans to resolve such conflicts.

BIBLIOGRAPHY

[1] Anca D. Dragan and Siddhartha S. Srinivasa, "A policy-blending formalism for shared control," *The International Journal of Robotics Research*, vol. 32, issue 7, pp. 790-805, 2013. https://doi.org/10.1177/0278364913490324

[2] J. Shervin, H. Admoni, S. Pellegrinelli, S. S. Srinivasa, and J. A. Bagnell, "Shared autonomy via hindsight optimization for teleoperation and teaming," *The International Journal of Robotics Research*, vol.37, issue 7, pp. 717-742, 2018. https://doi.org/10.1177/0278364918776060

[3] F. Semeraro, A. Griffiths, and A. Cangelosi, "Human-robot collaboration and machine learning: a systematic review of recent research," arXiv:2110.07448v4, 2022. https://doi.org/10.48550/arXiv.2110.07448

[4] A. Ajoudani, A. M. Zanchettin, S. Ivaldi, A. Albu-Schäffer, K. Kosuge, and O. Khatib, "Progress and prospects of the human–robot collaboration," *Autonomous Robots*, vol. 42, pp. 957–975, (2018). https://doi.org/10.1007/s10514-017-9677-2

[5] C. Basdogan, C. HO, M. A. Srinivasan, and M. Slater, "An experimental study on the role of touch in shared virtual environments," *ACM Trans. Comput-Hum. Interact.*, vol. 7, no. 4, pp. 443–460, 2000.

[6] J. Moll and E.-L. Sallnäs, "Communicative functions of haptic feedback," in *Proc. of the 4th International Conference on Haptic and Audio Interaction Design*, pp. 1–10, 2009.

[7] A. Kucukyilmaz, S. O. Oguz, T. M. Sezgin, and C. Basdogan, "Improving human-computer cooperation through haptic role exchange and negotiation," in *Proc. Immersive Multimodal Interactive Presence*, pp. 229–254, 2012.

[8] R. Groten, D. Feth, R. L. Klatzky, and A. Peer, "The role of haptic feedback for the integration of intentions in shared task execution," *IEEE Trans. Haptics,* vol. 6, no. 1, pp. 94–105, First Quarter 2013.

[9] G. Ganesh, A. Takagi, R. Osu, T. Yoshioka, M. Kawato, and E. Burdet, “Two is better than one: Physical interactions improve motor performance in humans,” *Sci. Rep.*, vol. 4, Art. no. 3824, 2014.

[10] A. Takagi, F. Usai, G. Ganesh, V. Sanguineti, and E. Burdet, “Haptic communication between humans is tuned by the hard or soft mechanics of interaction,” PLoS Comput. Biol., vol. 14, no. 3, pp. 1–17, 2018.

[11] A. Takagi, M. Hirashima, D. Nozaki, and E. Burdet, “Individuals physically interacting in a group rapidly coordinate their movement by estimating the collective goal,” *eLife*, vol. 8, Art. no. e41328, 2019.

[12] L. Marchal-Crespo, J. Furumasu, and D. Reinkensmeyer, “A robotic wheelchair trainer: design overview and a feasibility study,” J. *Neuro-Engineering Rehabil.*, vol. 7, no. 1, pp. 1–12, 2010.

[13] S. Parastegari, E. Noohi, B. Abbasi, and M. Žefran, “Failure recovery in robot-human object handover,” in *IEEE Trans. Robot.*, vol. 34, no. 3, pp. 660–673, Jun. 2018.

[14] E. A. Mielke, E. C. Townsend, and M. D. Killpack, “Analysis of rigid extended object co-manipulation by human dyads: Lateral movement characterization,” arXiv:1702.00733, 2017.

[15] E. Mielke, E. Townsend, D. Wingate, and M. D. Killpack, “Human robot co-manipulation of extended objects: Data-driven models and control from analysis of human-human dyads,” arXiv:2001.00991, 2020.

[16] E. Noohi and M. Žefran, “Quantitative measures of cooperation for a dyadic physical interaction task,” in *Proc. IEEE-RAS Int. Conf. Humanoid Robots*, pp. 469–474, 2014.

[17] N. Jarrass_e, V. Sanguineti, and E. Burdet, “Slaves no longer: Review on role assignment for human–robot joint motor action,” *Adaptive Behav.*, vol. 22, no. 1, pp. 70–82, 2014.

[18] K. B. Reed and M. A. Peshkin, “Physical collaboration of human-human and human-robot teams,” *IEEE Trans. Haptics*, vol. 1, no. 2, pp. 108–120, First Quarter 2008.

[19] N. Stefanov, A. Peer, and M. Buss, “Role determination in humanhuman interaction,” in *Proc. IEEE 3rd Joint EuroHaptics Conf. Symp. Haptic Interfaces Virtual Environ. Teleoperator Syst.*, pp. 51–56, 2009.

[20] A. Takagi, N. Beckers, and E. Burdet, “Motion plan changes predictably in dyadic reaching,” *PLoS One*, vol. 11, no. 12, Paper. e0167314, 2016.

[21] A. Melendez-Calderon, V. Komisar, G. Ganesh, and E. Burdet, “Classification of strategies for disturbance attenuation in human-human collaborative tasks,” in *Proc. Annu. Int. Conf. IEEE Eng. Med. Biol. Soc*., pp. 2364–2367, 2011.

[22] N. Jarrass_e, T. Charalambous, and E. Burdet, “A framework to describe, analyze and generate interactive motor behaviors,” *PLoS One*, vol. 7, no. 11, Paper e49945. [Online]. https://doi.org/10.1371/journal.pone.0049945

[23] Y. Li, G. Carboni, F. Gonzalez, D. Campolo, and E. Burdet, “Differential game theory for versatile physical human–robot interaction,” *Nature Mach. Intell*., vol. 1, no. 1, pp. 36–43, 2019.

[24] D. J. Agravante, A. Cherubini, A. Sherikov, P.-B. Wieber, and A. Kheddar, “Human-humanoid collaborative carrying,” IEEE Trans. Robot., vol. 35, no. 4, pp. 833–846, Aug. 2019.

[25] C. E. Madan, A. Kucukyilmaz, T. M. Sezgin, and C. Basdogan, “Recognition of haptic interaction patterns in dyadic joint object manipulation,” *IEEE Trans. Haptics*, vol. 8, no. 1, pp. 54–66, Jan.–Mar. 2015.

[26] A. Kucukyilmaz and I. Issak, “Online identification of interaction behaviors from haptic data during collaborative object transfer,” *IEEE Robot.* Autom. *Lett*., vol. 5, no. 1, pp. 96–102, Jan. 2020.

[27] T. Wojtara, M. Uchihara, H. Murayama, S. Shimoda, S. Sakai, H. Fujimoto, and H. Kimura, “Human–robot collaboration in precise positioning of a three-dimensional object,” *Automatica,* vol. 45, no. 2, pp. 333 – 342, 2009. https://doi.org/10.1016/j.automatica.2008.08.021

[28] G. Kang, H. S. Oh, J. K. Seo, U. Kim, and H. Ryeol Choi, “Variable Admittance Control of Robot Manipulators Based on Human Intention,” In *IEEE/ASME Transactions on Mechatronics*, vol. 24, no. 3, pp. 1023-1032, June 2019. https://doi.org/10.1109/TMECH.2019.2910237

[29] Y. Aydin, N. Arghavani and C. Basdogan, “A New Control Architecture for Physical Human-Robot Interaction Based on Haptic Communication,” *9th ACM/IEEE International Conference on Human-Robot Interaction (HRI),* pp. 122-123, 2014. http://dx.doi.org/10.1145/2559636.2563682

[30] A. Lecours, B. Mayer-St-Onge, and C. Gosselin, “Variable admittance control of a four-degree-of-freedom intelligent assist device,” *IEEE International Conference on Robotics and Automation*, pp. 3903-3908, 2012. https://doi.org/10.1109/ICRA.2012.6224586

[31] Y. M. Hamad, Y. Aydin, and C. Basdogan, “Adaptive Human Force Scaling via Admittance Control for Physical Human-Robot Interaction,” In *IEEE Transactions on Haptics*, vol. 14, no. 4, pp. 750-761, 2021. https://doi.org/10.1109/TOH.2021.3071626

[32] S. O. Oguz, A. Kucukyilmaz, T.M. Sezgin, and C. Basdogan, “Supporting negotiation behavior with haptics-enabled human-computer interfaces,” *IEEE Trans. Haptics*, vol. 5, no. 3, pp. 274–284, Third Quarter 2012.

[33] A. Kucukyilmaz, T. M. Sezgin, and C. Basdogan, “Intention recognition for dynamic role exchange in haptic collaboration,” *IEEE Trans. Haptics*, vol. 6, no. 1, pp. 58–68, First Quarter 2013.

[34] A. Mörtl, M. Lawitzky, A. Kucukyilmaz, M. Sezgin, C. Basdogan, and S. Hirche, “The role of roles: Physical cooperation between humans and robots,” *Int. J. Robot. Res.*, vol. 31, no. 13, pp. 1656–1674, 2012.

[35] M. Khoramshahi and A. Billard, “A dynamical system approach to task-adaptation in physical human–robot interaction,” *Autonomous Robots*, 43, pp. 927–946, 2019. https://doi.org/10.1007/s10514-018-9764-z

[36] M. Khoramshahi and A. Billard, “A dynamical system approach for detection and reaction to human guidance in physical human–robot interaction,” *Autonomous Robots*, 44, pp. 1411–1429, 2020. https://doi.org/10.1007/s10514-020-09934-9

[37] E. C. Townsend, E. A. Mielke, D. Wingate, and M. D. Killpack, “Estimating human intent for physical human-robot co-manipulation,” 2017. https://doi.org/10.48550/arXiv.1705.10851

[38] B. Whitsell and P. Artemiadis, “Physical Human–Robot Interaction (pHRI) in 6 DOF With Asymmetric Cooperation,” In *IEEE Access*, vol. 5, pp. 10834-10845, 2017. https://doi.org/10.1109/ACCESS.2017.2708658

[39] S. S. Ge, Y. Li, and H. He, “Neural-network-based human intention estimation for physical human-robot interaction,” *8th International Conference on Ubiquitous*

Robots and Ambient Intelligence (URAI), pp. 390-395, 2011. https://doi.org/10.1109/URAI.2011.6145849

[40] Y. Li and S. S. Ge, "Human–Robot Collaboration Based on Motion Intention Estimation," In *IEEE/ASME Transactions on Mechatronics*, vol. 19, no. 3, pp. 1007-1014, 2014. https://doi.org/10.1109/TMECH.2013.2264533

[41] B. Guler, P. P. Niaz, A. Madani, Y. Aydin, and C. Basdogan, "An adaptive admittance controller for collaborative drilling with a robot based on subtask classification via deep learning," *Mechatronics*, 86:102851, 2022. https://doi.org/10.1016/j.mechatronics.2022.102851

[42] W. Lu, Z. Hu, and J. Pan, "Human-Robot Collaboration using Variable Admittance Control and Human Intention Prediction," *IEEE 16th International Conference on Automation Science and Engineering (CASE)*, pp. 1116-1121, 2020. https://doi.org/10.1109/CASE48305.2020.9217040

[43] K. T. Ly, M. Poozhiyil, H. Pandya, G. Neumann, and A. Kucukyilmaz, "Intent-Aware Predictive Haptic Guidance and its Application to Shared Control Teleoperation," *IEEE International Conference on Robot & Human Interactive Communication (RO-MAN)*, pp. 565-572, 2021. https://doi.org/10.1109/RO-MAN50785.2021.9515326

[44] S-H. Chien, J-H. Wang, and M-Y. Cheng, "Robotic Assistance for Physical Human–Robot Interaction Using a Fuzzy RBF Hand Impedance Compensator and a Neural Network Based Human Motion Intention Estimator," In *IEEE Access*, vol. 9, pp. 126048-126057, 2021. https://doi.org/10.1109/ACCESS.2021.3111875

[45] W. Wang, R. Li, Y. Chen, and Y. Jia, "Human Intention Prediction in Human-Robot Collaborative Tasks," In *Companion of the 2018 ACM/IEEE International Conference on Human-Robot Interaction (HRI '18). Association for Computing Machinery*, New York, NY, USA, pp. 279–280, 2018. https://doi.org/10.1145/3173386.3177025

[46] D. Sirintuna, I. Ozdamar, Y. Aydin, and C. Basdogan, "Detecting Human Motion Intention during pHRI Using Artificial Neural Networks Trained by EMG Signals," *29th IEEE International Conference on Robot and Human Interactive Communication (RO-MAN)*, pp. 1280-1287, 2020. https://doi.org/10.1109/RO-MAN47096.2020.9223438

[47] F. Babel, J. M. Kraus, and M. Baumann, "Development and Testing of Psychological Conflict Resolution Strategies for Assertive Robots to Resolve Human-Robot Goal Conflict," *Front Robot AI*, Vol. 7, Article 591448, 2021. https://doi.org/10.3389/frobt.2020.59144

[48] L. Breiman, "Random forests," *Mach. Learn*., vol. 45, no. 1, pp. 5–32, 2001.

[49] S. Garrido-Jurado, R. Muñoz-Salinas, F. J. Madrid-Cuevas, and M. J. Marín-Jiménez, "Automatic generation and detection of highly reliable fiducial markers under occlusion," *Pattern Recognit.*, vol. 47, no. 6, pp. 2280–2292, 2014.

[50] F. Pedregosa, G. Varoquaux, A. Gramfort, V. Michel, B. Thirion, O. Grisel, M. Blondel, P. Prettenhofer, R. Weiss, V. Dubourg, J. Vanderplas, A. Passos, D. Cournapeau, M. Brucher, M. Perrot, and É. Duchesnay, "Scikit-learn: Machine Learning in Python," *Journal of Machine Learning Research*, vol. 12, pp. 2825–2830, 2011. https://doi.org/0.5555/1953048.207819

[51] O. Khatib, "Real-time obstacle avoidance for manipulators and mobile robots," In *Proceedings of the IEEE Conference on Robotics and Automation*, pp. 500-505, 1986. https://doi.org/10.1109/ROBOT.1985.1087247

[52] Z. Al-Saadi, D. Sirintuna, A. Kucukyilmaz, and C. Basdogan, "A Novel Haptic Feature Set for the Classification of Interactive Motor Behaviors in Collaborative Object Transfer," In *IEEE Transactions on Haptics*, vol. 14, no. 2, pp. 384-395, 2021. https://doi.org/10.1109/TOH.2020.3034244

[53] Y. Aydin, O. Tokatli, V. Patoglu, and C. Basdogan, "Fractional order admittance control for physical human-robot interaction," *IEEE World Haptics Conference (WHC)*, pp. 257–262, 2017. https://doi.org/10.1109/WHC.2017.7989911

[54] A. Madani, P. P. Niaz, B. Guler, Y. Aydin, and C. Basdogan, "Robot-Assisted Drilling on Curved Surfaces with Haptic Guidance under Adaptive Admittance Control," *IEEE/RSJ International Conference on Intelligent Robots and Systems (IROS)*, pp. 3723-3730, 2022. https://doi.org/10.48550/arXiv.2207.13999